Journal of Asian Earth Sciences 255 (2023) 105760

Contents lists available at ScienceDirect

Journal of Asian Earth Sciences

journal homepage: www.elsevier.com/locate/jseaes

Structure and kinematics of active faulting in the northern domain of Western and Central Alborz, Iran and interpretation in terms of tectonic evolution of the region

Ahmad Rashidi [a,b,*], Majid Nemati [a,c], Shahram Shafieibafti [c], Shahrokh Pourbeyranvand [b], Reza Derakhshani [c,d], Carla Braitenberg [e]

[a] Department of Earthquake Research, Shahid Bahonar University of Kerman, Kerman 7616913439, Iran
[b] International Institute of Earthquake Engineering and Seismology, Tehran 1953714515, Iran
[c] Department of Geology, Shahid Bahonar University of Kerman, Kerman 7616913439, Iran
[d] Department of Earth Sciences, Utrecht University, 3584 CB Utrecht, Netherlands
[e] Department of Mathematics and Geoscience, University of Trieste, 34127 Trieste, Italy

ARTICLE INFO

Keywords:
Active fault zone
Earthquake hazard
Strain partitioning
Transpressional zone
Tectonic geomorphology
Alborz
Northern Iran

ABSTRACT

Field evidence, seismicity, and geodetic data are combined to define the tectonic evolution along the northern domain of the Western and Central Alborz ranges, which have experienced significant earthquakes. One of our main focuses is to present the geometric-kinematic characteristics of active fault planes in the North Alborz fault zone and its subsidiary faults as a basis for seismic hazard assessment. To evaluate the seismotectonics in the region, three active segments of the seismic zone are identified. These segments primarily exhibit reverse mechanisms and left-lateral strike-slip components and act as the boundaries of neotectonic stress domains around the transition zone between Alborz and the South Caspian Basin. The spatial distribution of the strike-slip and dip-slip faulting over the Western and Central Alborz range supports our understanding of the geodynamic processes of the region. Our map of local active faults reveals five main systems with N–S, NE–SW, ENE–WSW, E–W, and NW–SE directions. Field studies indicate that strike-slip movements predominate and are consistent with a ~WNW-ESE-oriented left-lateral wrench system. Pure left-lateral strike-slip faults trending E-W, extensional faults trending NE–SW, and compressional faults trending NW-SE are identified. Regional field investigations reveal spatial variations in the fault zone width of the northern domain of the Western and Central Alborz. The findings demonstrate that fault zone structures and their spatial distribution along the width of the area are strongly affected by the strain partitioning process in the transpressional zone. A spectacular well-exposed transpressional zone from the Western and Central Alborz region is described in detail, where outer domains are faults with a dominant reverse mechanism, and the inner domain is a wrench zone that includes faults with a dominant strike-slip mechanism.

The seismic activity in the Northern Alborz region is mainly concentrated along the North Alborz fault zone and its subsidiary fault planes, of which some are identified for the first time in this research. Significant seismic events have occurred at locations where these newly identified fault planes interact. The maximum values of the geodetic strain axes in Western and Central Alborz are consistent with the area of high seismicity.

1. Introduction

Northern Iran is a tectonically intensly active region, as demonstrated by the strong and frequent earthquakes in the Alborz- Talesh mountain ranges and the South Caspian Basin (SCB) (Ambraseys and Moinfar, 2010; Tatar et al., 2007; Berberian and Yeats, 2001; Priestley et al, 1994; Berberian et al, 1992; Ambraseys and Melville, 1982). The destructive earthquakes in northern Iran from 1953 to 2021 have caused ~54,810 human casualties and ~168.5 km of fault surface ruptures (Rashidi and Derakhshani, 2022). Due to the unknown geometric- kinematic characteristics of the faults on the northern domain of the Alborz mountain range, fault rupture hazard assessment is not

* Corresponding author at: Bahonar University of Kerman, Kerman, Iran.
E-mail address: rashidi@uk.ac.ir (A. Rashidi).

https://doi.org/10.1016/j.jseaes.2023.105760
Received 23 February 2023; Received in revised form 22 May 2023; Accepted 14 June 2023
Available online 19 June 2023

accurate, and the determination of structural parameters of the active faults provides important data required for a realistic interpretation of seismotectonic observations. The Alborz mountain range has a V-shaped geometry and contains faults with NE-SW and NW-SE orientations in its eastern and western parts, respectively (Fig. 1). The style of the overall deformation has been defined through a system of double-verging folds, left-lateral strike-slip, and reverse faults which are sub-parallel to the range (Berberian, 1983; Stöcklin, 1974).

The kinematics of the North Alborz fault zone, and its branches, such as the NW-SE Royan fault zone, and NNE-SSW trending minor active faults, have not been accurately identified based on field evidence. Their characteristics are known mostly based on satellite images (e.g., Nazari et al., 2021; Rashidi, 2021; Allen et al., 2003).

Some important earthquakes in the region (e.g., the 2004 May 28 Baladeh earthquake; Mw 6.2) are the result of the activity of the North Alborz fault zone and its branches (e.g., Royan fault) (Rashidi, 2021). Although various researchers have linked numerous earthquakes to the North Alborz fault, no surface seismic rupture has been reported on the fault (Nazari and Ritz, 2008). Some researchers believe that this fault has been active since the Silurian (Nabavi, 1976). Considering the long history of its formation and its activity, the width of the North Alborz fault zone is noteworthy, reaching about 15 km in parts of the region..

This research aims to demonstrate that the poorly characterized northern domain of the Western and Central Alborz structural zone in northern Iran experiences significant deformation. Previous studies have mostly relied on satellite and DEM (Digital Elevation Models) images as well as the distribution of earthquake epicenters to identify active fault planes and define the structural map of Iran (e.g. Nazari et al., 2021; Rashidi, 2021; Tatar et al., 2007). In the study geomorphological field work has been made to map the faults.

Tectonic geomorphology has emerged as a crucial tool in various applications, such as the reconnaissance of active faults, fault rupture hazard assessment, investigation of landscape evolution, and identification of geological structures. This tool's effectiveness lies in the recognition of distinct landforms shaped by tectonic forces, which have been generated and preserved over observable time scales, providing valuable insights into geological processes (Derakhshani et al., 2023; Dayal, 2010; Keller and Pinter, 2002).

The ability to map active faults on the ground surface and study their tectonic geomorphology depends strongly on the amount and type of

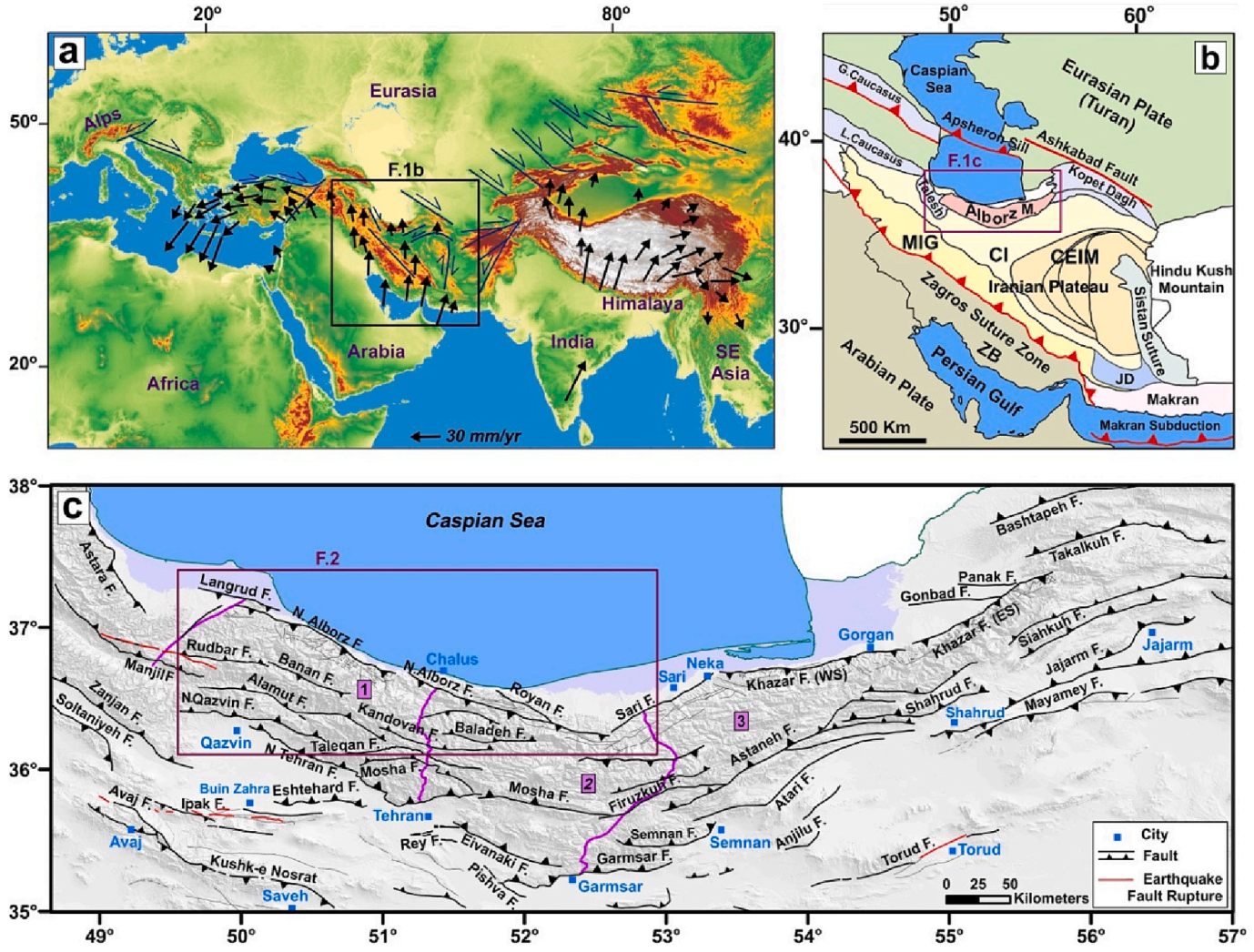

Fig. 1. Tectonic and Geographic location of the study region. (a) Topography (SRTM30) of the Alpine-Himalaya orogenic belt resulted from the collision of the Eurasian plate with the African, Arabian, and Indian plates. The velocity vectors are relative to the Eurasian reference frame (determined by Vernant et al. (2004)). (b) The regional structure of the continental collision of Eurasia–Arabia and the location of the Alborz mountain range and its surrounding region in northern Iran. Abbreviations: CEIM = Microcontinents of the Central-East Iranian; CI = Central Iran; MIG = Metamorphic Rock Zone and Intruded Granitoides; JD = Jazmurian Depression; ZB = Zagros Belt. (c) Faults of Alborz and surrounding region (the faults are from (Rashidi, 2021; Hessami et al., 2013; Sheykholeslami et al., 2013). The purple frame shows the location of Fig. 2, which includes the North Alborz fault system. Numbers 1, 2, and 3 are the positions of the Western, Central, and Eastern Alborz, separated by purple lines. (For interpretation of the references to color in this figure legend, the reader is referred to the web version of this article.)

vegetation (Rashidi et al., 2021; Tsereteli et al., 2016; Walker et al., 2010). In arid regions (e.g., the Wadi Araba basin in Egypt; the Gobi - desert in NW China; the Lut desert in eastern and southern Iran), we can describe the faults with a level of detail that is not possible in the humid region. However, in the humid area, most of the tectonic geomorphic features are obscured due to the dense vegetation, as are forest covers (e. g., Tsereteli et al., 2016; De Pascale et al., 2016; Chen et al., 2015; Selim et al., 2013; Goswami et al., 2009). Therefore, studies of the active tectonics in the region with dense vegetation- forest as the Alborz, have to involve lots of field visits, an approach described here.

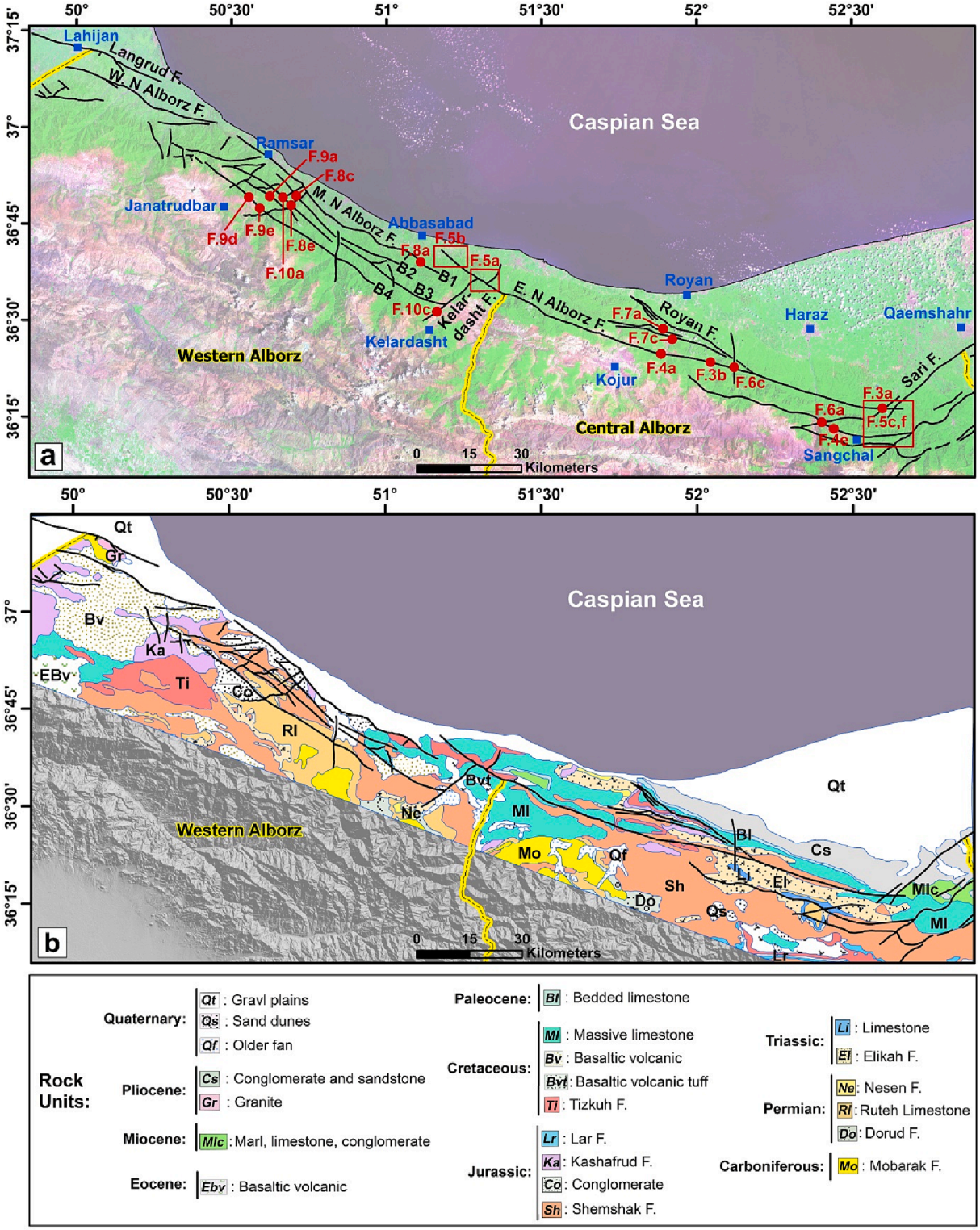

Fig. 2. Structural and geological maps of the northern domain of central and western Alborz. (a) The North Alborz fault zone with the location of the field evidence (red circle), DEM, and Satellite (Red Polygon) images which show the position of the next figures. Abbreviations: E. N Alborz F., M. N Alborz F., and W. N Alborz F. respectively are eastern segment, middle segments and western segment of the North Alborz fault zone. (b) The rock units and geological formations surrounding the North Alborz fault zone. (For interpretation of the references to color in this figure legend, the reader is referred to the web version of this article.)

Vegetation, forest cover, and erosive phases are the cause that not much information about the function of the different branches of the fault zone is uncovered. Therefore, in this study, we try to overcome this deficiency by conducting field visits throughout the length of this fault zone at different stations (Fig. 2). Various evidences converge to determine the geometric and kinematic characteristics of different branches of the eastern and middle segments of the fault zone. No suitable field evidence is found for the western segment.

Our findings indicate that seismogenic fault planes in regions of northern Iran covered by vegetation and forests have remained uncharacterized until now (Fig. 1). Further, we present detailed field evidence of fault planes of northern Iran integrated with the analysis of their seismicity and strain rate defined from the Global Positioning System (GPS) geodesy.

The subject is of current global interest due to the recent earthquake activity in the Anatolian Plate close to the study area (e.g. Barbot et al., 2023) and the need for more research on the relation between the plate boundaries and the earthquake activity in the region.

2. Geologic and tectonic setting

The Arabia-Eurasia collision zone is part of the Alpine-Himalayan belt, which is one of the youngest continental collisions on earth (Jackson et al, 1995) (Fig. 1a, b). The initial collision of the Eurasian and Arabian plates began in the late Eocene (Ballato et al., 2011) and accelerated in the Miocene (McQuarrie and Van Hinsbergen, 2013; Mouthereau et al., 2012; Allen et al., 2004). As structural deformations related to the collision zone gradually shifted to the intraplate regions such as the Alborz-Talesh range and Iranian Plateau sub-zones like Central Iran (Rashidi et al., 2023), they ultimately led to the subduction of the SCB plate beneath the Eurasian plate along the Aspheron sill (Fig. 1).

GPS surveys define the convergence rate of Eurasia – Arabia to ~22 mm/yr shortening in the N-S direction (Vernant et al., 2004). From this general rate, ~8 mm/yr is taken up in the Zagros range, ~3 mm/yr is accommodated in Central Iran, and ~5 mm/yr is consumed in the Alborz range. The SCB moves towards the NW with ~6 mm/yr, and left-lateral strike-slip shear throughout the Alborz is limited to ~4 mm/yr (Vernant, 2004). The SCB consists of a thick pile of sedimentary layers (Brunet et al., 2003), reaching ~20 km of sedimentary deposits, making it one of the deepest basins on earth (Brunet et al., 2003). These deposits overlie a thinner basement with high-velocity within the basin and a thicker basement around its southern domain (Mangino and Priestley, 1998). This basement may be thickened oceanic crust or thin continental crust (Jackson et al., 2002; Kadinsky-Cade et al, 1981).

The ~600 km long Alborz mountain range, as one of the oldest sub-zones in the region, has experienced various tectonic events, from the Cimmerian orogeny in the Late Triassic to the current-day stages of the Arabia–Eurasia convergence (Trifonov et al., 2022; Berberian and King, 1981; Şengör and Kidd, 1979). The Cimmerian orogeny resulted from the collision with Eurasia of the Gondwana fragment Cimmeria which affected the Eurasian domain from Turkey to Thailand (Şengör, 1984; Stöcklin, 1974). The Alborz in Late Cretaceous presents different facies differentiated from east to west, comprising granitoid intrusions to the west of central Alborz, and carbonate series in Central Alborz (Berberian and Berberian, 1981). In the northern domain of Alborz, Paleocene marine deposits are visible, including volcanic rocks in the west, while the Eocene formations are not seen. Anyway, in younger sedimentary deposits, reworked relics of the Eocene fauna demonstrate that Eocene units had been eroded after the Oligocene orogenic uplifts (Ghassemi, 1990), activated by the Arabia collision with Iranian terranes (Davoudzadeh and Weber-Diefenbach, 1997).

The Alborz range, which is divided into the three Eastern, Central, and Western parts, has a current-day deformation that is governed by significant left-lateral strike-slip and reverse faults, sub-parallel to the range trend (e.g., Jackson et al., 2002; Berberian, 1983) (Fig. 1c). The right-lateral strike-slip component along the W-NW faults which are related to the tectonic events before Pliocene, have been only identified in the Central and Western Alborz (e.g., Ballato et al., 2013; Landgraf et al., 2009; Allen et al., 2003). The main faults of the Alborz range with a current- day dominant thrust mechanism are found at the northern (such as North Alborz and Khazar faults) and southern (such as Jajarm, Garmsar, and North Tehran faults) margins of the orogen, while the dominant left-lateral strike-slip mechanism is localized inside the range (such as Rudbar, Mosha, Taleghan faults) (Fig. 1c). Therefore, strain partitioning is the present deformation mechanism in the range (Jackson et al., 2002), with left-lateral strike-slip (~3 and ~7 mm/yr, for the west and east of the Alborz range, respectively) and reverse faults (~6 and ~2 mm/yr, for the west and the east of the Alborz range, respectively) (Djamour et al., 2010; Mohammadi Nia et al., 2023).

Faulting in the northern domain of the range is difficult to distinguish because of the poor exposure, and few studies have been fulfilled in the region (Ghassemi, 2005), indicating some evidence for folding and active thrusting along the Khazar fault zone (Fig. 2), which confirms Berberian's (1983) suggestion about the ~3 km thrust motion along the Khazar fault. The proposed geologic profiles by Huber and Eftekhar-nezhad (1978a,1978b) in the Central Alborz indicated no evidence of surface outcrop of south-dipping thrusts. Rashidi (2021) characterized the northern domain of the Alborz by four main fault zones: the Langrud, the North Alborz, the Sari, and the Khazar fault zones from west to east, respectively. Fault reviewing in the northern domain of the Alborz range indicated that the Khazar fault joins to the north Alborz fault by an oblique ramp (the Sari fault) (Rashidi, 2021). In other words, the Khazar fault in the eastern Alborz is the continuation of the North Alborz fault in the Central and Western Alborz (Rashidi, 2021). In parts of its length, the North Alborz fault zone has thrusted the Paleozoic and Mesozoic formations onto the Neogene formations (Saidi et al., 2003). It has been proposed that the North Alborz fault zone is a deep-rooted fault from the late Precambrian to the present (e.g., Nazari, 2006). Tatar et al. (2007) identified an aftershock of the 2004 Baladeh earthquake delineating a rupture zone with a south dip-direction between 15 and 30 km depth beneath the northern domain of the Central Alborz. The rupture zone of the Baladeh earthquake intersects the ground surface trace of one of the branches of the North Alborz fault (Royan fault), as inferred by Rashidi (2021) (Fig. 2). Therefore, the North Alborz fault zone is the most important active fault zone in the Western and Central Alborz (Fig. 2) which has not been studied in detail in the field.

The 300-km-long North Alborz fault zone is located in the south-western part of the SCB and on the northern domain of the western and central Alborz mountain range (Fig. 1), from south of Lahijan city in the west to the Sangchal village in the east (Fig. 2). The fault zone consists of three main segments of the western, middle and eastern Alborz, with lengths of ~145, ~100 and ~55 km, respectively (Fig. 2). Folds related faults have been identified in the middle fault segment (Rashidi, 2021). According to Stöcklin (1974), the fault zone has experienced more than two kilometers displacement in the Pliocene to Pleistocene. The fault zone has cut the geological formations of different ages. Along parts of the length of fault planes, the Precambrian-Paleozoic formations of the northern margin of the range have been placed next to the Quaternary sediments of the SCB (Nabavi, 1976). Also, this fault zone has put the Mesozoic sedimentary rocks on top of the Cenozoic rocks. So, it marks the southernmost boundary of the Neogene deposits of the SCB (Rashidi, 2021; Stöcklin, 1974).

The current-day configuration and faults distributions with different mechanisms in the Alborz had been accompanied by a change in the stress direction from N-S to NE-SW in Pliocene (Allen et al., 2003; Jackson et al., 2002). Various studies have been done on strain rate for the Iranian plateau and its structural sub-zones (e.g., Rashidi et al., 2022; Mehrabi et al., 2021; Raeesi et al., 2017; Zarifi et al., 2014; Masson et al., 2004). Recent studies of the strain and stress fields in northern Iran indicated ~N35.5°E as the mean stress direction for the Alborz (Rashidi and Derakhshani, 2022).

3. Materials and methods

To define the seismotectonics of the North Alborz fault zone, we integrate detailed geological evidence with seismologic and geodetic data. Mapping and delineation of tectonic geomorphological features related to the North Alborz fault zone are commonly obscured because of the dense vegetation, including forest covers, human modifications of the geomorphological traces, and severe water erosion. So, the aerial photographs, DEM models, satellite imagery (such as Landsat, Aster, Quickbird), visualized in Google Earth, and Indian Remote Sensing (IRS) data are investigated with the aim to to determine fault lineaments and site selection for fieldwork on each plane of the fault zone.

Fault kinematics and active tectonic studies of the region are fulfilled using a survey of the deformations in the Quaternary landforms and rock units, investigating the tilting and cumulative offsets of the phenomena related to the fault activities, structural indicators of fault planes in the field and earthquake focal mechanisms.

The characteristic faults are mapped through direct field recognition and applying classical methods and instrumentation including tiltmeter, compass, and goniometer. To measure the pressure (P) and extension (T) quadrants for the fault planes with kinematic indicators such as the slicken-lines, and also to obtain the positions of the principal-stress axes (σ1, σ2, and σ3) (e.g., Ezati et al., 2022), we use the FaultKin Linked Bingham distribution software (Allmendinger, 2001). We refer to the relevant publications for the data processing and methodological details.

The simultaneous use of geomorphological evidence of tectonics, seismic catalogs, and geodetic data (e.g., Rashidi et al., 2022c) lets us define the fault ability to generate seismic events with a specific magnitude and return period. For this purpose, we investigate the distribution of instrumental earthquakes from the various catalogs such as IIEES (International Institute of Earthquake Engineering and Seismology), IGUT (Institute of Geophysics, the University of Tehran), Engdahl Bulletin (Engdahl et al., 2006) and Master Event Relocation Technique (MLoc) catalogue (https://seismo.com). The seismological networks allow us to determine fault dip and fault outcrop through the aftershock distribution of the 1990 Rudbar – Tarom earthquake (Rezapour, 1991; Tatar and Hatzfeld, 2009) and the 2004 Baladeh event (Tatar et al., 2007) in Central and Western Alborz. Several authors (Tatar et al., 2012; Nemati et al., 2011; Abbassi et al., 2010; Abbassi et al., 2005) deployed local networks to survey background seismicity in the south and east of Alborz, respectively.

In some cases, the geometric and kinematic characteristics of active fault planes obtained in the field can be confirmed using reliable earthquake focal mechanisms. A number of the focal mechanisms in the Alborz have been computed in different studies (e.g., Tatar et al., 2007; Jackson et al, 1995; Priestley et al, 1994; Akasheh and Berckhemer, 1984). Some other reliable solutions are found in the Centroid Moment Tensor catalogue (GCMT Harvard).

The GPS velocity vector data is derived from selected stations concentrated in the study region from one of the previous studies in Iran (Khorrami et al., 2019). 10 years long data series from the IPGN (the Iranian Permanent GNSS Network), in addition to the published velocity vectors from GPS studies, are combined in the present dataset. Geodetic strain rates are estimated from the GPS velocity vectors using the Haines and Holt method (Beavan and Haines, 2001; Holt et al, 1995). The observed velocity field can be parameterized by using a rotation vector function at the surface of a sphere. This rotation vector function can then be expanded on a curvilinear grid using bi-cubic Bessel interpolation (Keiding et al., 2015).

4. Structural features

The North Alborz fault zone forms the northern margin of the western and central Alborz mountain range. Its eastern termination striking ~N85°W in the eastern Alborz laterally juxtaposes to the Khazar fault through the Sari fault with a strike of ~N50°E (Rashidi, 2021). Based on DEM and satellite images, the western end of the fault zone, with a strike of ~N80°W, terminates ten kilometers southwest of Lahijan city (Fig. 2). According to the field evidence and analysis of the DEM and Satellite images, the fault zone can be divided into three main segments: the eastern, middle, and western segments (Fig. 2).

4.1. The eastern segment of the North Alborz fault zone

This segment includes three sub-parallel fault branches in the eastern part of central Alborz (Fig. 2), where the left-lateral displacements of the stream beds are observed (Fig. 3a). Along its northern branch where its attitude is N50°W, 50°SW (Fig. 3b), the Cretaceous rock units are thrusted on each other. The younger planes of the fault branch with attitudes of N75°W, 45°SW, and N75°W, 20°SW can be seen within Pliocene units (Fig. 3c, d). Our field data of the fault planes with attitudes of N85°W, 50°SW, and slicken-line of 240°/35° propose a left-lateral strike-slip mechanism with a reverse component for the fault zone (Fig. 3e, f) where the fault has an east–west trend and is linked to the NE-SW Sari fault.

In the middle part of the eastern segment of the North Alborz fault zone, in geographical location of 51.85°E, 36.40°N, the outcrop of the northern branch of the fault zone is clearly observable (Fig. 4a). In this point, the Jurassic shales on the hanging wall of low- angle faults (dipping < 30°) are thrusted on the Jurassic limestone units (Fig. 4b). The steeper fault planes with attitude of N70°W, 75°SW and their slicken-lines (234°/72°) suggest reverse mechanism with left-lateral strike-slip component for the eastern segment of the North Alborz fault zone (Fig. 4c, d).

There are no field and satellite evidences of the western continuations of the two southern branches (see the Fig. 2). These branches in the eastern part of the central Alborz, in many parts of their length, are located within and between the Triassic (e.g. Elika) and Jurassic (e.g. Shemshak) formations (Fig. 2a). In the field visits of the fault where the fault trace with the trend of N70°W is visible, overturned folds are observed on the fault hanging wall (Fig. 4e, f). The folds of the region emphasize the important role of the reverse component of the fault branches during their activity. Considering these folds are on Mesozoic units and are associated with older deformation events, we can consider that the area has been subject to deformation, at least from the late Cretaceous.

The western part of the eastern segment of the North Alborz fault zone is formed by a narrow fault zone with a visible trace on the IRS satellite images (Fig. 5a) where on its hanging-wall, the Cretaceous Limestone and Marls rock units with left-stepping en-echelon pattern have been uplifted (Fig. 5b). The structural map of the region shows the eastern and middle segments of the North Alborz fault zone follow a left-stepping en-echelon pattern. The western terminus of their northern branches interacted with the shorelines of the Caspian sea (Fig. 2).

In the field visits of the fault zone (eastern segment), several minor active faults were found. Our data reveal the minor faults with attitudes of N90°E, 70°S, and striations of 266°/10° (Trend/Plunge) have left-lateral strike-slip mechanisms (e.g., Fig. 5c, d). Geometric and kinematic characteristics of other minor fault planes (N60°E, 80°SE; 060°/05°) within the fault zone show a left-lateral strike-slip mechanism with normal component (Fig. 5e, f).

In the northern domain of the Alborz mountain range, several N-S and NE-SW faults have cut off the eastern segments of the North Alborz fault zone. For example, within Triassic- Jurassic rock units, the fault with an attitude of N75°E, 45°SE has cut off the southern branch of the fault zone (in the geographical location of 52.40°E, 36°N), and has formed the folds-related fault (e.g., Fig. 6a) where the fault trace is visible on the field images (e.g., Fig. 6b). In another point (52.10°E, 36.40°N), the faults with an attitude of N00°E,70°E, and slicken-lines of 035°/65° which show right - lateral strike-slip mechanism with a reverse component, has cut off the northern branch of the fault zone (Fig. 6d, e).

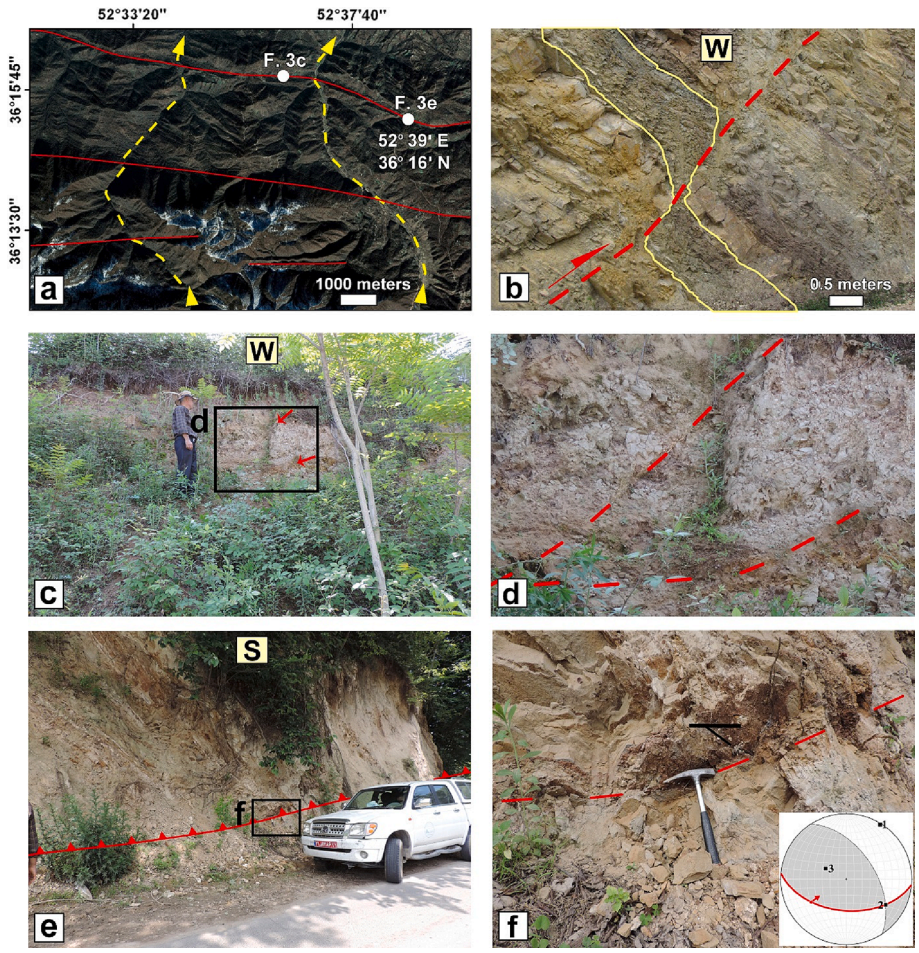

Fig. 3. Three branches of the eastern segment of the North Alborz fault zone (a) and the field evidence of its northern branch (b–f). (a) Quickbird image (from Google Earth) of traces of the three fault branches and left-lateral offsets of the streams. (b) Reverse offset of the sedimentary rock units on the fault plane (modified after Hessami (2017)). (c) Fault traces within the Pliocene sandstone and conglomerate. (d) Close-up view of the faults of Fig. 3c) with attitudes of N75°W, 45°SW and N75°W, 20°SW. (e) The fault trace with attitude N85°W,50°SW. (f) Close-up view of the slicken-line traces (240°/35°) on the fault plane of Fig. 3e).

At this point, low - dipping fault planes have formed folds related faults (e.g., Fig. 6e) within the Elika and Shemshak formations.

4.1.1. Royan fault zone

The 60 km long Royan fault zone, based on satellite images, was introduced for the first time by Rashidi (2021). In this study, we present field evidence of the geometric and kinematic characteristics of this important and little- known fault zone in the Central Alborz (see the fault location in Fig. 2). The WNW-ESE Royan fault zone created various geological structures such as folds-related faults (Fig. 7). It is possible that some documented earthquakes on the northern domain of the Central Alborz (e.g., the 2004 May 28 Baladeh earthquake) have been related to the recent activity of the Royan fault zone (Rashidi, 2021). The fault zone, which consists of three main branches, has cut the Kashafrud, Tizkuh, Shemshak, and Elika geological formations (see Fig. 2).

Field survey at location 51.90°E, 36.50°N indicated that the branches of the Royan fault zone with an attitude of N70°W, 65°SW, and striation of 254°/52° have a reverse mechanism with a left-lateral strike-slip component (Fig. 7a, b). At this point, the Royan fault zone is located between the Elika formations to the north and the Shemshak formation to the south. Southern branches of the Royan fault zone at locations 51.90°E and 36.40°N have created anticlines-related fault activities (Fig. 7c–f). At this point, most of the fault branch is located between Shemshak and Kashafrud formations.

4.2. The middle segment of the North Alborz fault zone

This segment includes four parallel fault branches where the width of the fault zone is about ten kilometers (B1 to B4 in Fig. 2a). The northern branch and three southern branches, respectively, are located in the foothills and mountains. This study provides the surface traces and the geometric and kinematic characteristics of these branches for the first time.

Along the northern branch of the fault zone with an attitude of N50°W, 45°SW (B1 on Fig. 2), the Tizkoh formation is thrusted over the Quaternary sediments (Fig. 2b). The crushing of the rock units on the hanging wall and folds related faulting have been special structural features along the northern branch (e.g., Fig. 8a, b). Considerable shortening in the region has caused the folds to break around their axial planes and to generate faults with attitudes of N60°W, 85°SW (Fig. 8b).

We investigate the structural characteristics of the three southern branches of the North Alborz fault zone in the south of Ramsar (see the location in Fig. 2). In the location 50.65°E, 36.80°N, the second branch of the fault zone (B2 in Fig. 2) with attitude N70°W, 65°SW and striations of 265°/10° has a reverse mechanism with a left-lateral strike-slip component (Fig. 8b, c). This fault has separated the Shemshak formation from the Jurassic conglomerate. In 50.60°E, 36.75°N, the third branch of the fault zone (B3 in Fig. 2) separates the Ruteh formation to the north from the Shemshak formation to the south (Fig. 2b). This branch of the fault zone with an attitude of N50°W, 60°SW, and striations of 256°/55° show a reverse mechanism with a left-lateral strike-slip component (Fig. 8e, f).

The western continuation of the third branch of the fault zone (B3 in Fig. 2) with a left-step arrangement can be followed in the Shemshak and Ruteh formations (Fig. 2b). Folds-related fault activities have formed in these rock units. We measure the geometric characteristics of the fault planes (Fig. 9a-c). At location 50.60°E, 36.70°N, the principal planes of

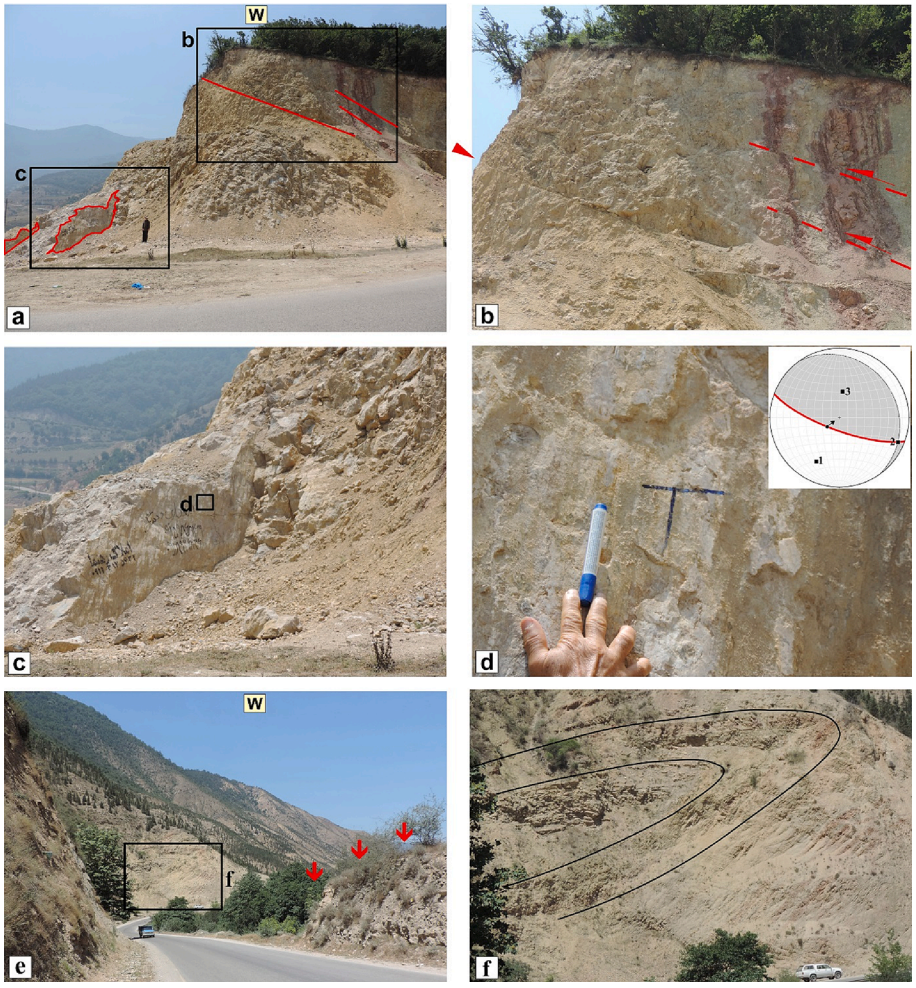

Fig. 4. The field evidence of the northern and middle branches of the eastern segment of the North Alborz fault zone. (a) Outcrop of the planes of the northern branch with various dips. (b) Close-up view of the reverse offsets on the low-dipping fault planes. (c) The steeper fault planes with an attitude of N70°W, 75°SW. (d) Close-up view of the slicken-line (234°/72°). (e) Trace of the middle fault branch with a trend of N70°W and overturned fold on the fault hanging wall. (f) Close-up view of the overturned fold.

the fault branch have an attitude of N40°W, 60°SW and N40°W, 40°SW with a back thrust plane of N40°W, 65°NE (Fig. 9a).

The southernmost branch of the North Alborz fault zone (B4 in Fig. 2) is named Lir-e Sar fault (Sheykholeslami et al., 2013). This fault branch has formed folds related to fault activity (e.g., Fig. 9d). The fault plane with an attitude of N50°W, 50°SW can be seen within the Jurassic conglomerate (e.g., Fig. 9e, f). Along this fault branch, Permian rock units (e.g., Ruteh formation) are thrusted over the Jurassic rock units (e.g., Shemshak formation).

In our field visits of the middle segment of the North Alborz fault zone, the NE-SW minor active faults were identified. These faults with an attitude of ~N25°E, 80°SE, and striations of ~200°/25° have a right-lateral strike-slip mechanism and normal components (e.g., Fig. 10a, b). The minor faults interacted with some branches of the middle segment where those have cut and shifted Ruteh, Elika, and Shemshak formations throughout its length.

No particular field evidence was found for the western continuation of the middle segment of the fault zone. But, for its eastern continuation, the fault zone is connected to the Kalardasht fault zone with an attitude of ~N55E, 60SE (Fig. 2). The dip-slip mechanism of the Kalardasht fault zone can be measured in parts of its length. So, in the northwest of Kalardasht city (51.15°E, 36.50°N), the normal offsets of the sedimentary layers are observed on the planes of the fault zone (Fig. 10c), such that some planes show ~4 m normal offset of the layers (Fig. 10d).

5. Seismicity of the Alborz mountain range and the North Alborz fault zone

The Alborz mountain range is uplifted, as a result of the Arabian-Eurasian plates convergence, through a system of double-verging faults. One of the main northern verging fault is the North Alborz faults zone. The current- day mechanism of the faults in the Alborz are mainly reverse and left lateral strike slip, which accommodate respectively normal and oblique crustal movements of central Iran and SCB relative to Alborz. Moho depth, and therefore seismogenic thickness in Alborz, is strongly variable from north to south and also from west to east across the Alborz range. According to a tomography profile in the western Alborz, Moho depth varies from 40 to 45 km from north to south (Motaghi et al., 2018). In the eastern Alborz, Nemati et al. (2012) computed the Moho depth ~35 km as average, which correlates with the eastern Alborz width. The Moho depth in the Central Alborz (Abbassi et al., 2010), and beneath the Damavand summit (Sodoudi et al., 2009) is 51–58 km and ~68 km, respectively.

Alamut, North Qazvin, Banan, and Kandvan faults in the central and western Alborz don't show significant seismicity, while Khazar, North Alborz fault, Mosha, Astaneh, Garmsar are seismically active with mainly moderate seismicity (Fig. 11). Historical earthquakes are missing along the North Alborz fault zone except for its eastern part where it interacts with the Sari fault (Fig. 11). However, in the southern domain and east of Alborz, there are many strong earthquakes along the various active faults in the historical period (Fig. 11a). It seems that missing historical earthquakes in the north of Alborz in seismicity maps are not related to a realistic seismic gap in the historical era, but instead might

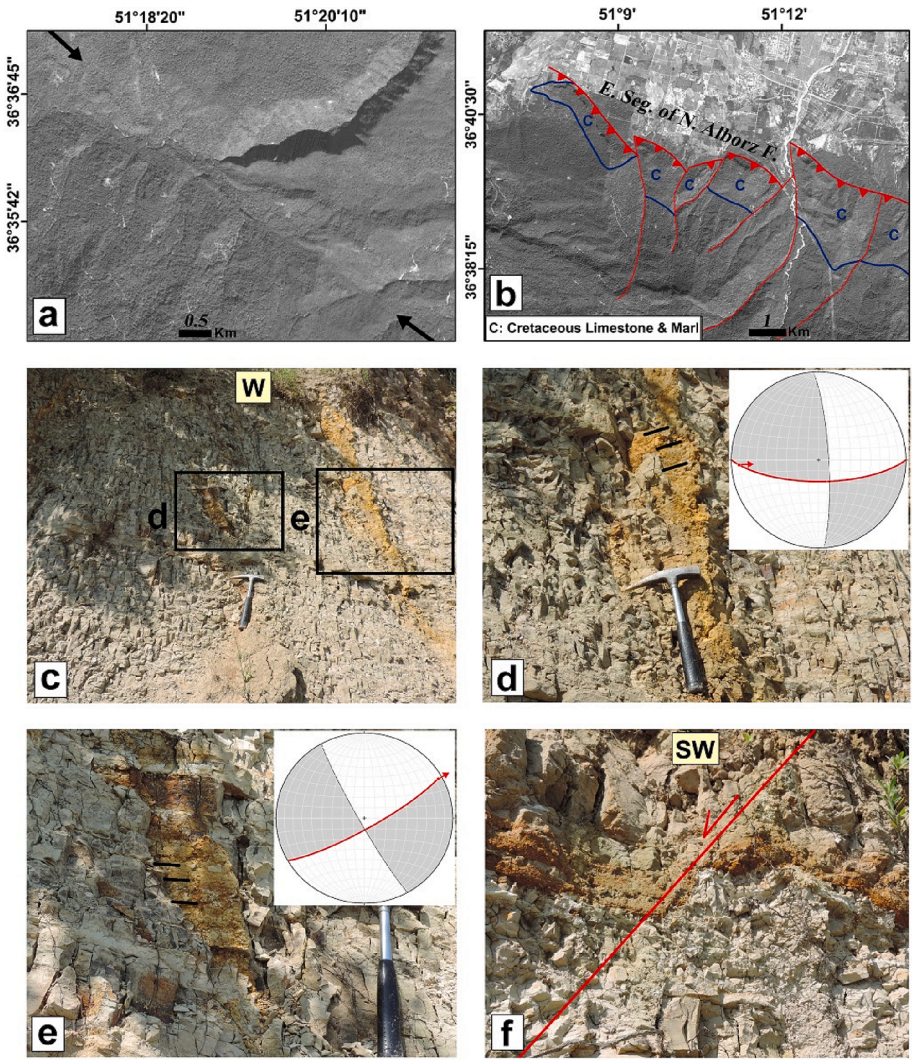

Fig. 5. Trace of the western part of the eastern segment of the North Alborz fault zone on the IRS satellites (a, b), and structural characteristics of its minor branches (c–f). (a) Fault trace in the western part of its length. (b) Western terminus of the eastern segment with a left-stepping en-echelon pattern where the Cretaceous Limestones and Marls have been uplifted on the hanging wall. (c) The minor fault planes within the Pliocene sandstone and conglomerate. (d) Close-up view of the fault plane with an attitude of N90°E,70°S, and slicken lines of 266°/10°. (e) Close-up view of the fault plane with an attitude of N60°E,80°SE, and slicken lines of 060°/05°. (f) Normal offset within the Pliocene sandstone and conglomerate along the minor fault with an attitude of N60°E, 80°SE.

be due to a minor infrastructural development in this region in the past. Reporting of historical events in the south strongly depends on inhabitants that lived south of Alborz in ancient cities like Caspian and Qumesh (current Qazvin) and Damghan cities, respectively (Kosarev and Kostiany, 2010). According to the distribution pattern of the instrumental earthquakes from the Institute of Geophysics, University of Tehran (IGUT), the seismic activity in the Alborz has mainly been concentrated near Astaneh, Firuzkuh, Mosha, Rudbar, North Alborz faults and less associated with Garmsar, and Khazar faults (Nemati et al., 2011). Because of the appropriate spacing between the IGUT stations in Alborz in recent years, earthquake locations are precise enough to study the fault geometry and compute focal mechanisms. Instrumentally recorded seismicity has a fairly precise location in Alborz. Teleseismic locations are accurate to about 15 km for magnitude completeness of Mw $\geq$ 5.5 (Engdahl et al., 2006), which is not sufficient to study seismicity at the scale of an active fault, and only a few events have been relocated in the region. The other earthquake data set with reliable location accuracy is the Master Event Relocation Technique (MLoc) catalogue (https://seismo.com). This catalogue is not complete and is mainly based on aftershocks of large earthquakes rather than background seismicity. For example, this catalogue is limited to only a few clusters of events. The clusters are Baladeh – Shahmirzad- Rudbar, and Mosha clusters, which are based on the 2004 (M_W 6.4) Baladeh earthquake and 1990 (M_W 7.7) Rudbar – Tarom earthquake (Berberian et al, 1992; Berberian and Walker, 1990), respectively. They do not cover all of the Alborz region. Local seismological network recordings are a reasonable and, therefore, reliable database for active fault investigations. This data has the potential to determine precise outcrops of the active faults and the dip in seismic sections. In Alborz, there are a few seismological networks: aftershock surveying of the 1990 Rudbar -Tarom earthquake (Rezapour, 1991; Tatar and Hatzfeld, 2009) and the 2004 Baladeh event (Tatar et al., 2007). Background seismicity in the southern domain and east of Alborz respectively, has been monitored by local networks (Nemati et al., 2011; Abbassi et al., 2010; Tatar et al., 2007; Abbassi et al., 2005). The authors of the networks realized that the North Alborz and Khazar faults are dipping ~40° southward, and Garmsar, North Tehran, Astaneh, Firouzkuh, and Mosha faults, as well as the Rudbar coseismic fault, are dipping near to vertically.

Based on the concept of tectonic indentation (Hoffman, 1987), the Caspian crust's indentation into the western Alborz range is expected to generate sinistral earthquake mechanisms along the northern domain of the Alborz (Jackson et al., 2002), which is confirmed by the focal mechanisms of a large number of earthquakes in this region. The 1990 Rudbar-Tarom (Berberian and Walker, 1990) earthquake (left-lateral strike-slip mechanism) and the 2004 Baladeh earthquake (reverse mechanism with left-lateral strike-slip component) are indicative of significant tectonic activity in the western Alborz seismotectonic province. These two events are the largest instrumental earthquakes ever recorded in the province.

The seismicity in the northern domain of Alborz is concentrated in

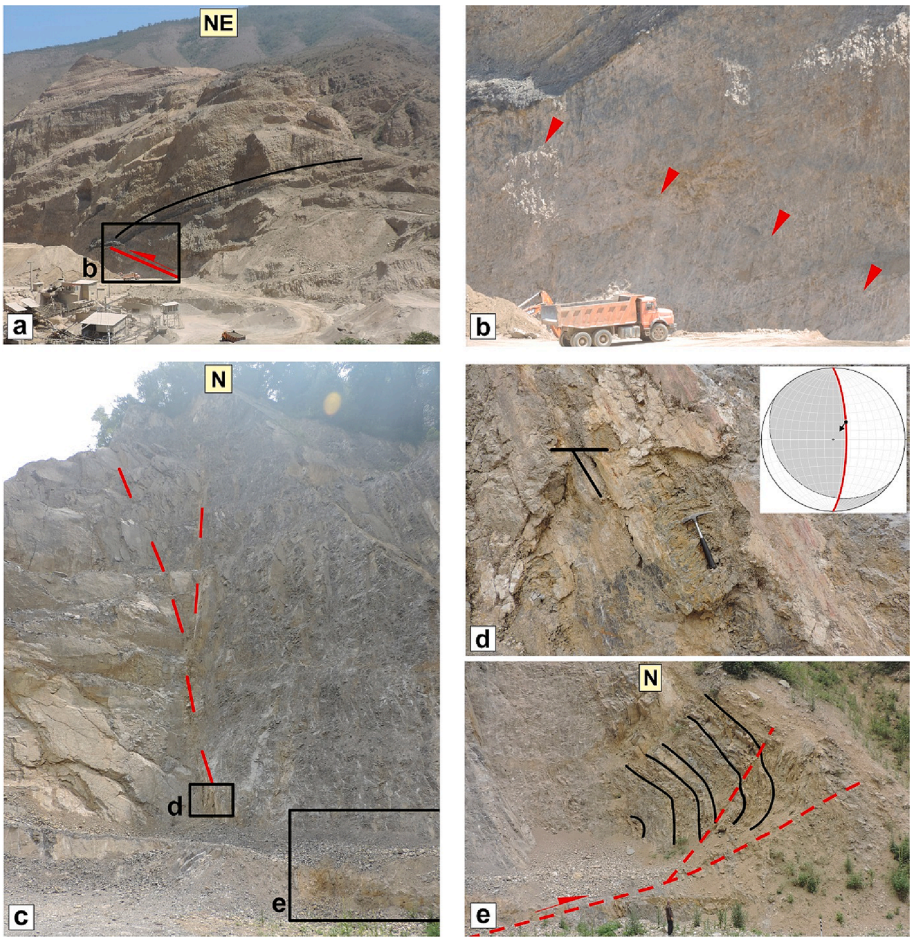

Fig. 6. Structural characteristics of the minor faults along the eastern and middle segments of the North Alborz fault zone. (a) The minor fault with an attitude of N75°E, 45°SE, which interacted with the southern branches of the fault zone. (b) Close-up view of the minor fault trace. (c) The minor fault interacted with the northern branch of the fault zone. (d) Close-up view of the minor fault plain with an attitude of N00°S, 70°E, and slicken lines of 266°/10°. (e) The faults-related folds that interacted with the northern branch of the fault zone.

the North Alborz and Khazar faults and their branches. Three categories of earthquakes could be associated with the North Alborz fault, in accordance with seismological networks data in Iran: micro-earthquakes data of the IGUT with detection of events with magnitude less than M 4.0, moderate earthquakes with magnitude between M 4.0 and M 5.5 and large earthquakes with magnitudes greater than M 5.5 (Fig. 11b).

According to the IGUT network data (between 2006 to present), the some of the largest observed earthquake in the Alborz was ~M 5 (2020/05/07) on the Mosha fault, and the largest events on the North Alborz fault were ~M 5.0 and ~M 4.7, which occurred in 2012/01/11 and 2017/12/05, respectively.

The mechanisms of earthquakes in Fig. 11a are adapted from GCMT, IIEES, IRSC, and ZUR_RMT catalogues (Table 1). The largest earthquakes with known mechanisms, which could be related to the North Alborz fault, are the 1998/12/03 M_W 5.4 dominantly reverse event (western segment of the fault) and also the 2004/05/28 M_W 6.4 reverse earthquake (Royan fault). Tatar et al. (2007) reported that the 2004 Baladeh earthquake, which had a reverse mechanism with a left-lateral strike-slip component, occurred at a depth of 22 km for the centroid depth (Donner et al., 2013). The earthquake is a microplate margin event involving the interaction between the SCB and Alborz regions based on its depth, faulting location, and low-stress drop. This information is consistent with the findings by Nemati (2015). Ballato et al. (2015) used the geometry of this event to estimate rock-uplift rates due to estimated shortening across the fault.

6. Geodetic strain rate in the Western and Central Alborz

Geodetic strain rate tensors in the study region are calculated from the published GPS station velocities, which are relative to the Eurasian reference frame (Khorrami et al., 2019) using the Haines and Holt method (Beavan and Haines, 2001; Holt et al, 1995) (Fig. 12a, Table 2). The direction and magnitude of the principle axes of the strain rate tensor show important variations throughout the region. To illustrate the variation in the direction of the principle strain axes, a modified version of the new method proposed by Pourbeyranvand (2021) is used in this study. The direction of the principal strain rate axis is represented by a specific color based on an innovative 2D color scale (Fig. 12b). Furthermore, a contour scheme of the orientation of the compressional strain rate axis is introduced and added to the output figure, to deal with the ambiguity arising from the limited capability of human vision to infer slight differences in colors.

The direction of the principal strain rate axis gains further interest when compared with the fault trends and orientations since the geodetic strain rate determines the fault movement or slip on the fault plane.

Based on the geodetic results presented in Fig. 12, the tectonic regime in the region is transpressive. Most regions have a green color, which shows the overall or background deformation direction is ~NE-SW, as expected due to the general compressional tectonic forces and the convergence between Arabia and Eurasia. But due to the implementation of the new mapping method, some anomalies in strain rate principle axes directions are observed for the first time.

It should be mentioned that the resolution of the image obtained in Fig. 12b is directly related to the GPS velocity vector data as the input to the strain rate study. This means that the uncertainties in the obtained strain rate tensor axes affect the resolution of the direction variation. The resolution of the image is 0.2 deg following the strain rate calculation parameters. In this circumstance, the anomalies affect the nearby grid cells and may have produced some artifacts that may not precisely coincide with the real geological features in the vicinity of the strong

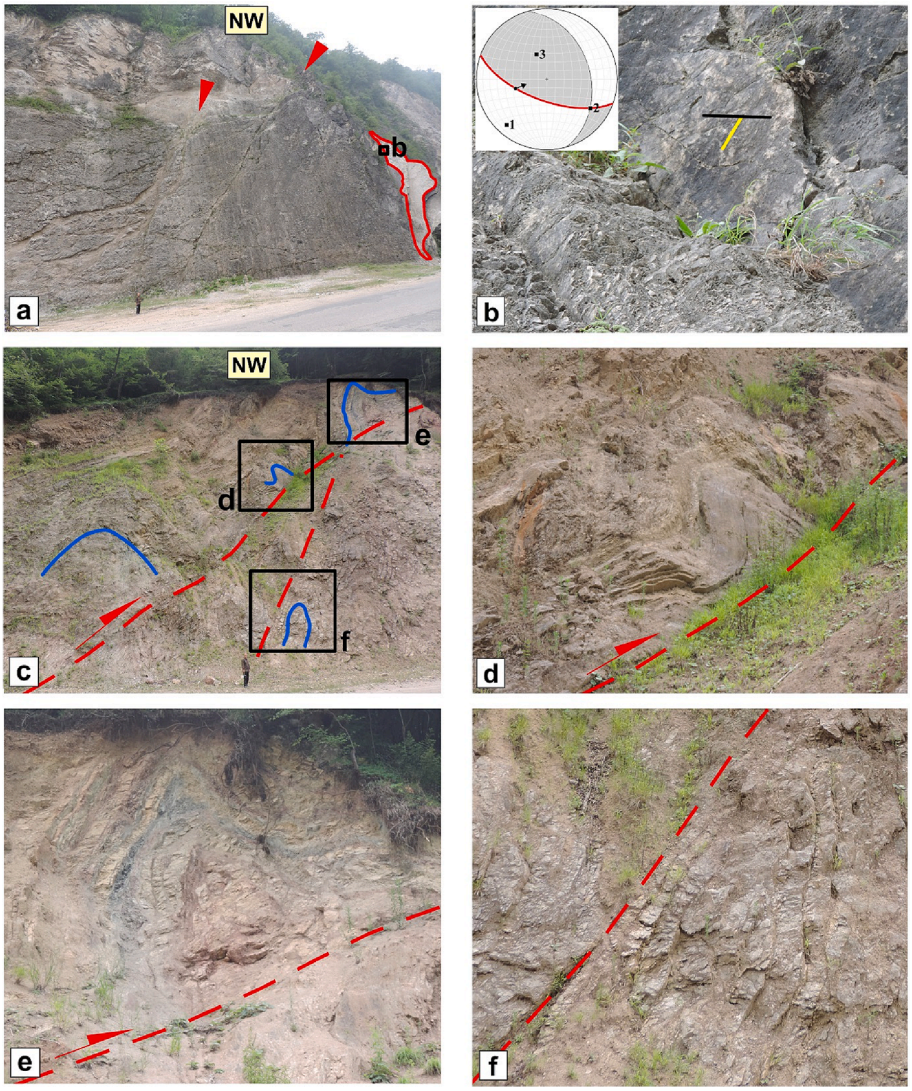

Fig. 7. Structural characteristics of the Royan fault zone. See Fig. 2 for the location of the Royan fault zone. (a) Traces of the fault planes at location 51.90°E, 36.50°N. (b) Close-up view of the fault plane with an attitude of N70°W, 65°SW, and striation of 54°/52°. (c) The southern branch of the Royan fault zone with anticlines-related fault activities at location 51.90°E, 36.40°N. (d, e, and f) Close-up view of the anticlines-related fault activity.

anomalies. It is important to interpret the method's results with this consideration.

Fig. 12 displays the strain rate axes with perpendicular bars, where the cyan bar represents the negative strain rate or compressional axis, and the magenta bar represents the positive strain rate or extensional axis. In contrast to the 1D color scale used in traditional colored maps, the proposed method uses a 2D color scale. The map includes yellow contour lines that describe the azimuth direction of the compressional strain rate axes, with positive directions from north to east. The contour lines have a 25-degree interval between successive lines, and degree numbers are displayed in black on the lines. Faults in the region are also plotted in black. The legend of the map shows the color variation pattern that represents the direction of the cyan bars, which depict the principal axis of compressional deformation. Notably, the background color of the map changes with the direction of the cyan bars representing the compressional deformation axis.

The most prominent feature is observed in the center of the map, showing a nearly N-S direction around the Tehran region within the 25-degree contour. However, the uncertainty of the results means that the anomaly fades out within a few cells away from the center. Another interesting anomaly can be seen on the west side of the previously discussed anomaly around Tehran, within the 125 and 100-degree contour lines. On the east side of the red anomaly in the center of the map, a blue anomaly representing NW-SE strain rate compressional axes is visible.

Several other strong anomalies can be observed at the edges of the map, but the sources of these are placed outside of the study region. There are also some weak anomalies, but their difference in background color hardly exceeds the uncertainty or resolution threshold in the mapped data. Thus we limit the observed anomalies to the above-mentioned ones, and the investigations will be focused on those in the discussion part.

In Fig. 12b and Table 3, the magnitudes of the strain rate axes are also shown. The magnitude of the strain rate axes is higher in the eastern (right) part and southeastern (lower right) parts of the map. These axes are also longer in the western part of the map (lower left). The magnitudes of the strain rate axes are small in the middle of the map. In some cases, the magnitude of one of the axes is so tiny that it is not visible. In these cases, the direction of the cyan axis is still influential in defining the color of the cells according to the circular legend.

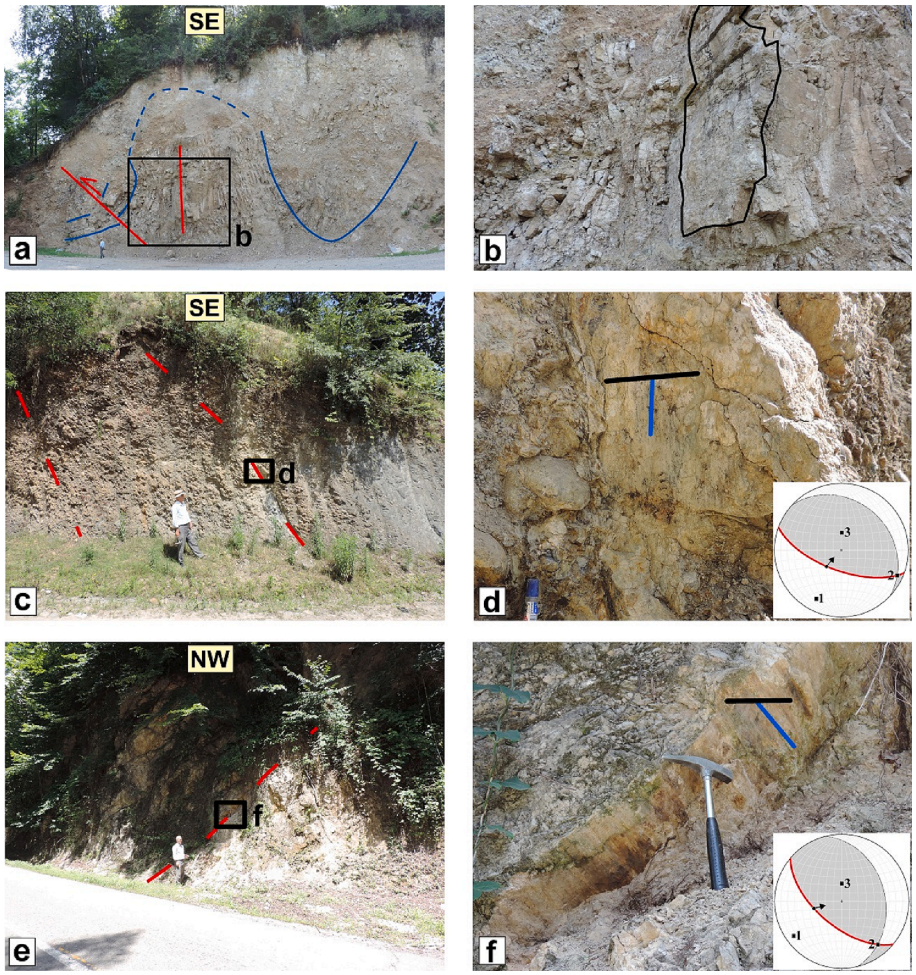

Fig. 8. Structural characteristics of the three northern branches (B1, B2, and B3) of the middle segment of the North Alborz fault zone (see the location of the fault branches in Fig. 2a). (a) Northern branch of the middle segment of North Alborz fault zone (B1) with an attitude of N50°W, 45°SW, and anticline related fault activity. (b) Close-up view of the fault with an attitude of N60°W, 85°SW around the axial plane of the anticline. (c) Traces of the second branch of the fault zone (B2) in the 50.65°E, 36.80°N. (d) Close-up view of the fault plain with an attitude of N70°W, 65°SW, and striations of 265°/10°. (e) Trace of the third branch of the fault zone (B3) at location 50.60°E, 36.75°N. (d) Close-up view of the fault plain with an attitude of N50°W, 60°SW, and striations of 256°/55°.

7. Discussion

7.1. Structural analysis of the study area

This research provides field evidence of activities on faults in the northern domain of the Alborz mountain range (e.g., North Alborz fault segments, Royan fault, Kalardasht fault) (Fig. 2). In seismic hazard assessment, each of these faults must be considered as a potential source of damaging earthquakes. We emphasize that the fault planes we present in the region (e.g., the Royan fault) have been sources for some of the large instrumental and historical earthquakes in the past centuries. The high sharp scarps along the fault planes in a region of alluvium can indicate the surface ruptures of different seismic events.

These faults are also significant for realizing how tectonic deformations are accommodated using faults, both on the local scale (at the northern domain of the Western and Central Alborz), and at the regional scale in the oblique structural zone (at the Western and Central Alborz range). Although the left-lateral strike- slip components of some fault branches are seen at several sites, we propose that the general motions at the northern domain of the range are oblique reverse. The eastern tip of the North Alborz fault in the Central Alborz laterally juxtaposes with the Khazar fault through the Sari fault (See Fig. 1c and 2a). According to the North Alborz and Khazar fault mechanisms (reverse mechanisms with left-lateral strike- slip components), an extensional zone has been generated along the Sari fault zone (read details in Rashidi, 2021). The western tip of the North Alborz fault and the Langrud fault with a right step pattern has created a local- transpressional deformation zone in the northwestern domain of the Western Alborz (read details in Rashidi, 2021).

Most kinematics of the North Alborz fault planes has been dominated by reverse and left-lateral strike-slip faulting, confirmed by our geodetic data. The direction change of the stress field before the Pliocene has led to the kinematic change of the faults in the Western and Central Alborz (Ballato et al., 2013; Landgraf et al., 2009). The dynamic source which has specified kinematics and geometry of faults in the region is collision of the SCB with Central Iran subzones within the Arabia- Eurasia convergence zone.

Over the past decades, most tectonic studies have been focused on the faults of the inner zone and southern domains of the Alborz (e.g., Talebian et al., 2016; Ghassemi et al., 2014; Nazari et al., 2014; Ritz et al., 2012; Rizza et al., 2011; Javidfakhr et al., 2011; Solaymani Azad et al., 2011; Nazari et al., 2009; Hollingsworth et al., 2008; Ritz et al., 2006), while few studies have dealt with the faulting of the northern domain of the Alborz due to the vegetation - forest covers (e.g., Nazari et al., 2021; Rashidi, 2021). The studies have indicated that the range not only accommodates crustal shortening deformation but also absorbs left-lateral strike-slip faulting. GPS evidence during decadal measurements also showed the oblique deformation along the Alborz range, especially in the Western and Central Alborz (Djamour et al., 2010; Vernant, 2004).

The North Alborz fault zone is not a uniform singular fault zone but instead includes three main segments called the western, middle, and eastern segments, with different lengths, strikes, and mechanisms. The western, middle, and eastern segments include two, four, and three main fault planes, respectively. Based on satellite images, geomorphological evidence of the activity of the eastern and western segments has been

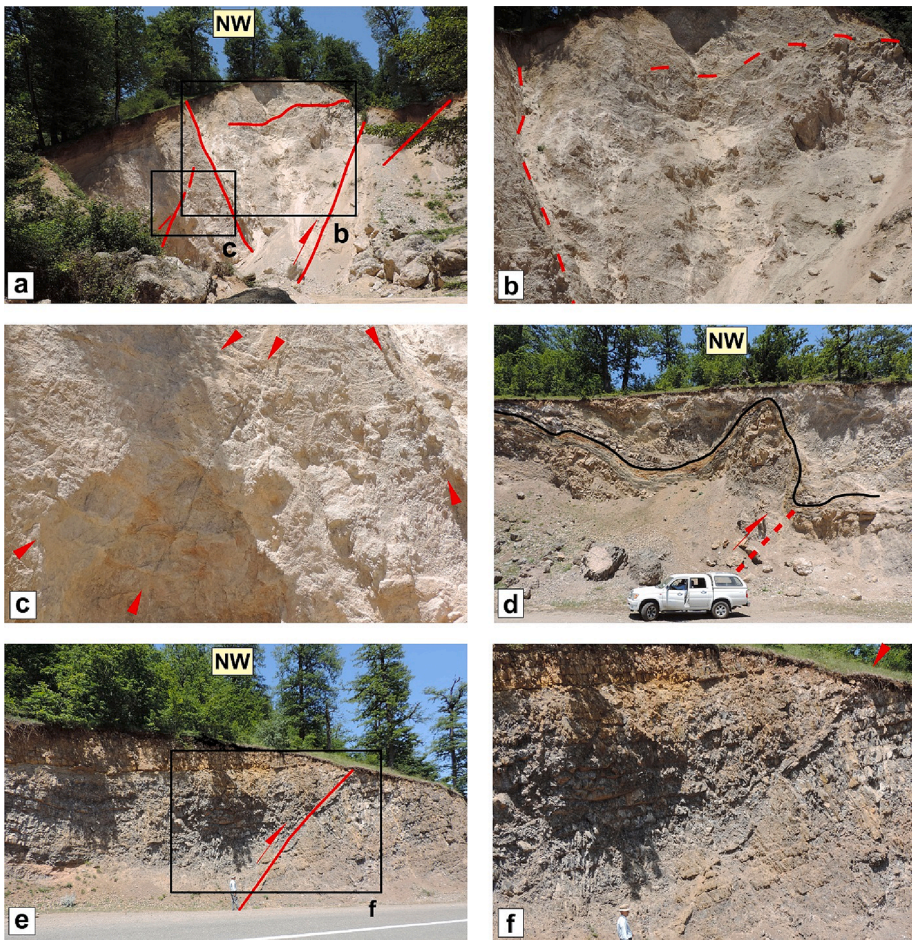

Fig. 9. Structural characteristics of the third and fourth branches of the middle segment of the North Alborz fault zone (B3 and B4 on Fig. 2). (a) The different planes of the third branch of the fault zone (B3). (b, c) Close-up view of the fault traces. (d) Folds-related faults along the southern branches of the fault zone (B4). (e) Plane of the fourth branch of the fault zone with an attitude of N50°W, 50°SW. (f) Close-up view of the fault plane within the Jurassic conglomerate.

presented by Rashidi (2021). The presented evidence has shown reverse mechanism and left-lateral strike-slip components as the current-day motions of the eastern segment (Rashidi, 2021), confirmed by our field visits in this study. In this study, we obtain the geometric and kinematic characteristics of all fault planes related to the eastern and middle segments of the North Alborz fault zone, which can be used as primary data in the seismic hazard assessment. Based on the field evidence and satellite images, the western segment of the North Alborz fault zone has a left-lateral strike-slip and reverse mechanism (Rashidi, 2021). Each of these fault segments includes subsidiary faults with different strikes and mechanisms. For example, the NW-SE Royan and the NE-SW Kalardasht faults have reverse (main component) and normal mechanisms, respectively.

7.2. Seismological analysis of the Alborz region

The Alborz range has experienced some moderate to large instrumental earthquakes, such as the 1935 Mw 6.8 Kusut, 1957 Mw 7 Sangchal, 1980 Mw 6.6 Shirabad, 1990 Mw 7.3 Rudbar, and 2004 Mw 6.4 Baladeh (Tatar et al., 2007; Berberian and Yeats, 2001, 1999; Berberian et al, 1992; Tchalenko, 1975). Among the earthquakes, the 1990 left-lateral strike- slip event occurred at a depth of ~16 km (Berberian, 1997; Berberian et al, 1992), and the 2004 reverse event originated at a centroid depth of 22 km (Tatar et al., 2007) within the inner zone and northern domain of the Alborz range, respectively. These two earthquakes have occurred in places where historical earthquakes have not been reported (Fig. 12). Some large to moderate historical earthquakes have been reported in the Central Alborz (Ambraseys and Melville, 1982). Historically, the seismic events have several times destroyed the ancient sites in the southern domain of the Central Alborz and around Teheran (Iran's capital). The Eivanaki, Rey, and North Tehran faults (Fig. 1c) are known as the sources of historical events in 312–280 BCE (Ms ~ 7.6), 743 (Ms ~ 7.2), 855 (Ms ~ 7.1), 1177 (Ms ~ 7.2), and 1384 CE (Berberian and Yeats, 1999; Ambraseys and Melville, 1982).

In the eastern part of the Central Alborz, the other significant seismic event, such as the 1957/07/02 M 7 Band-E Pay, occurred where the NW-SE fault planes (e.g., North Alborz fault zone) interact with the NE-SW fault planes (e.g., Sari fault zone). In this region, moderate instrumental earthquakes (e.g., the 1971/08/09 M 5.2 and 1992/09/22 M 5.1 earthquakes) and some historical earthquakes (e.g., 1678 M6.5; 1805; 1809 M6.5; 1825 M6.5) have occurred. The 1990 Rudbar earthquake (Mw 7.3), which happened after the 1983 Mw 5.4 Charazeh earthquake, produced a left-lateral strike-slip surface rupture extending ~80 km. The Manjil reverse fault was probably reactivated during the 1983 Mw 5.4 Charazeh earthquake (Sarkarinejad and Ansari, 2015). The Manjil fault interacted with the Rudbar fault with a left-lateral strike-slip mechanism inside the seismogenic layer of ~16 km (Berberian, 1997; Berberian et al., 1992).

7.3. Geodetic analysis of the Alborz region

The strain rate field along the Alborz range is obtained using GPS (Global Positioning System) data (Fig. 12). Concerning the magnitude of the strain rates axes, it is evident that the region with high seismicity is

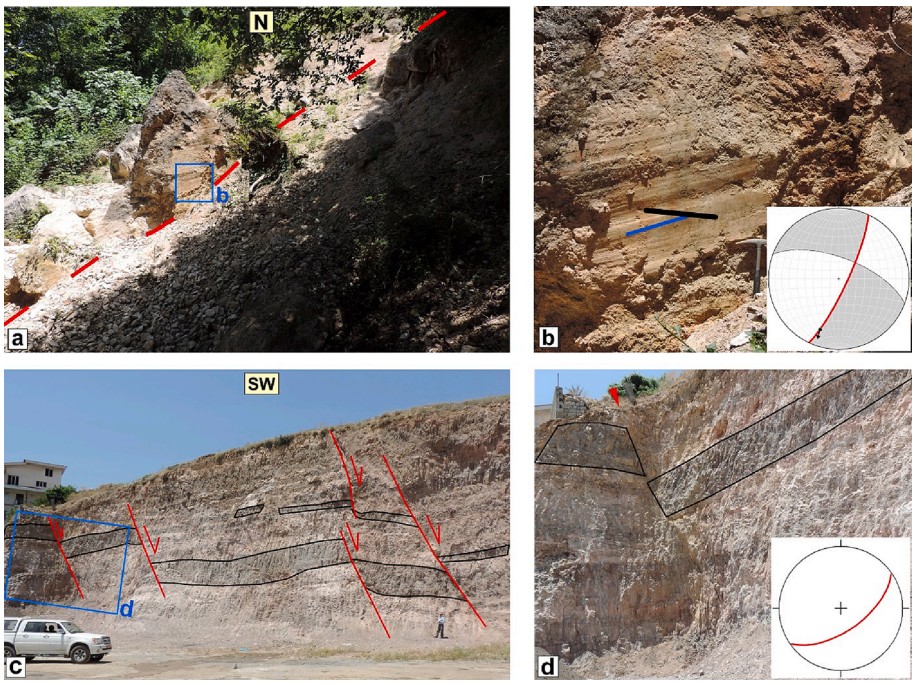

Fig. 10. Structural characteristics of the NE-SW minor active faults along the middle segment of the North Alborz fault zone. (a) The minor fault with the right-lateral strike-slip mechanism and normal component. (b) Close-up view of the fault plain with an attitude of N25°E, 80°SE, and striations of 200°/25°. (c) The normal offsets of the sedimentary layers along the planes of the Kalardasht fault zone. (d) Close-up view of the ~ 4 m normal offset along the western plane of the fault zone.

associated with greater strain rates. The large magnitude of both compressional and extensional axes of the principle strain rate coincides with high seismicity everywhere. Accordingly, regions with less seismic activity are distinguished with a lower magnitude of strain rate axes. The observation of both negative and positive strain rates resulting from geodetic deformation is caused by the acting tectonic forces. The presence of active faults in the brittle crust undergoing deformation can lead to seismic events.

For a detailed investigation of the fault orientations and their relationship with the strain rate axes, we need to focus on the anomalies discussed in the previous sections (Section 6; Fig. 12). For the anomaly in the center of the map (southern domain of the Western and Central Alborz; within 25-degree contour) the fault mechanism is predicted to be reverse, with a small strike-slip component. This prediction agrees with the overall tectonic regime and observations based on the previous studies in the region (Solaymani Azad et al., 2011; Tchalenko, 1975). The North Tehran fault is an example of the reverse mechanism. The low-temperature thermochronology data indicated that the North Tehran fault has been working as a master thoroughgoing, N-dipping reverse fault from ca. 7–6 Ma (Ballato et al., 2013). Based on the main principal geodetic axes, the reverse mechanism and left-lateral strike-slip component are the expected kinematics of the north Alborz fault zones as the northern domain of the Western and Central Alborz. As expected in the region's transpressive tectonic environment, some faults represent a strike-slip movement within the Alborz range. The Taleghan and the extension of the Mosha faults are cases related to this group.

Regarding the anomaly to the left, within the 125-degree contour placed on the Eshtehard fault, it is evident that the direction of the compressive strain rate axis is almost perpendicular to the fault orientation. Thus, the displacement mechanism on this fault is expected to be reversed, which is identical to the actual geological findings.

The anomaly to the right, within the 100-degree contour line, is located on a reverse segment of the Firuzkuh fault. This fault exhibits strike-slip motion at different locations to the right, towards its extension to the Astaneh fault, and to the left, towards the Mosha fault.

The along-strike changes in the convergence direction are due to the complex interaction between a local inhomogeneous stress field and variable orientations of the fault planes in the area. This has also happened during geological times, especially after Pliocene, and caused a variety of geologic structures as long-term deformation features.

Comparing the short-term deformation from GPS data, as performed here, and the long-term deformation from investigations on geological structures, including faults and folds, estimating the long-term component of shear strain rate values requires uplift and subsidence observation (Walcott, 1984). However, this is beyond the scope of this study and could be the subject of another independent research.

7.4. Regional tectonics and kinematic implications

This study describes the North Alborz fault zone as an active fault zone with reverse and left-lateral strike-slip motions along the northern domain of the Western and Central Alborz. The inner zone of Western and Central Alborz, which includes faults with left-lateral strike-slip mechanism (e.g., Rudbar and Mosha faults), is consistent with wrench deformation between parallel faults in the southern domain (e.g., North Qazvin, North Tehran, Eivanaki reverse faults) and northern domain. Several studies have been applied to show wrench deformation in the different areas of the ground surface (Mukherjee and Koyi, 2010; Jones et al., 2004; Sanderson and Marchini, 1984). However, there is the spatial separation of slip components onto parallel faults, with strike - slip inside the high mountains (inner zone) and shortening on the parallel faults at both the northern and southern domains of the high topography, but it does not appear as though this arrangement of faulting has persisted during the entire faulting history. So, in a general view of the region, our proposed model emphasizes a strain partitioning process in a transpression zone (Western and Central Alborz), whose outer domains are faults with a dominant reverse mechanism, and its inner zone is a wrench zone that includes faults with a dominant strike-slip mechanism (Fig. 13a). Based on the statistical calculation related to the stress regimes, Rashidi and Derakhshani (2022) confirm the slip partitioning process of oblique shortening within the Alborz. Types of transpression zones with various boundary wall orientations were presented by Dewey et al. (1998). Zone widening upwards between inward-dipping walls is consistent with the geometric features of the faults in

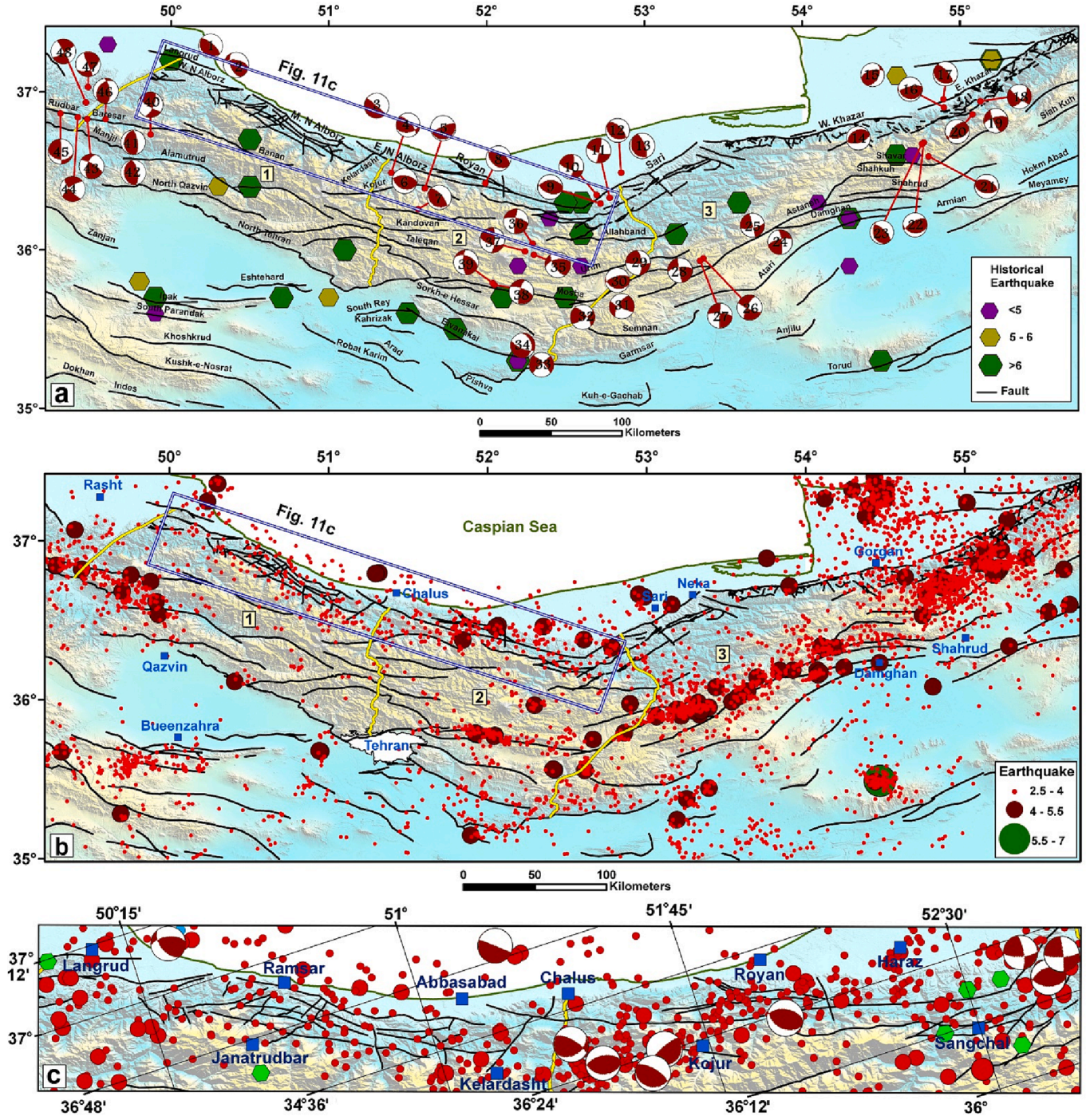

Fig. 11. Instrumental and historical earthquakes with some of the earthquake focal mechanisms and faults in the Alborz and their surrounding region. Numbers 1, 2, and 3 are, respectively, locations of the western Alborz, central Alborz, and eastern Alborz, which are separated by yellow lines. (a) The focal mechanisms of some earthquakes in the Alborz with historical earthquakes. Labels on the focal mechanism refer to the first column of Table 1. (b) Instrumental seismicity of the region after 2006 (from the IRSC). The blue frame shows the location of the North Alborz fault zone, which includes the most documented instrumental seismicity in the northern domain of Alborz after 2006. (For interpretation of the references to color in this figure legend, the reader is referred to the web version of this article.)

our study region.

A common feature of the transpressional zone is the inclined transpression model, which includes the simultaneous action of contraction and oblique-slip shear (Dewey et al, 1998; Harland, 1971). Transpression deformation zones have been identified in the southern Uplands of Scotland (Tavarnelli et al., 2004); the central Myanmar basin (Khin et al., 2021); the Zagros of Iran (Rahnama et al., 2008); Alborz in northern Iran (Nabavi et al., 2017). Based on the analog models, transpressional deformation such as simple transpression, transpression combined with the erosion of uplifted areas of the hanging wall above the deformation front, and transpression combined with the erosion of the hanging wall and sedimentation at the foot of uplifted zones have been presented by Casas et al. (2001).

The width of fault zones has been widely applied as a primary parameter in estimating total deformations (e.g., offsets), fault length and in understanding the tectonic evolution model of the region (e.g., Takagi et al., 2012; Sibson, 2003; Cowie & Scholz, 1992; Sibson, 1977). Brittle fault zones are usually determined using damage-zone structures,

Table 1
Parameters of the earthquake source (φ1, δ1, and λ1 symbols represent strike, dip, and rake angles of the preferred nodal planes, respectively) in Alborz. The first column label refers to the focal mechanisms in Fig. 11. Lat. and Long. refer to EHB (Engdahl bulletin), IIEES (International Institute of Earthquake Engineering and Seismology), and IRSC (Iranian Seismological Center). Abbreviations of References label: GCMT (Global Centroid Moment Tensor); ISC (Instrumental Earthquake Catalogue); ZUR_RMT (Zurich Moment Tensors); UPIES (moment tensors, University of Potsdam, Germany).

Label	Date (y/m/d)	Time	Lat.	Long.	Mag. (Mw)	Dep. (km)	Strike (φ1)	Dip (δ1)	Rake (λ1)	Reference
1	1980.07.22	5:17:08	37.322 (EHB)	50.262 (EHB)	5.6 (EHB)	25 (EHB)	135	20	95	GCMT
2	1980.12.03	4:26:13	37.126 (EHB)	50.43 (EHB)	5.3 (EHB)	16 (EHB)	160	52	136	GCMT
3	2004.05.29	9:23:49	36.488 (EHB)	51.396 (EHB)	4.7 (EHB)	14 (EHB)	185	3	145	ZUR_RMT
4	2004.05.28	12:38:45	36.259 (EHB)	51.566 (EHB)	4.5 (EHB)	25 (EHB)	76	40	35	ZUR_RMT
5	2004.05.28	13:35:56	36.39 (IIEES)	51.61 (IIEES)	4.4 (IIEES)	28 (IIEES)	75	13	98	UPIES
6	2012.07.27	21:39:03	36.896	51.3	4.3	8.5	276	56	81	(IIEES. Ya)
7	2004.05.28	19:47:05	36.426 (EHB)	51.398 (EHB)	6.4 (EHB)	27 (EHB)	119	24	72	GCMT
8	2002.04.08	18:30:55	36.422 (EHB)	51.992 (EHB)	4.8 (EHB)	9 (EHB)	134	42	104	ZUR_RMT
9	1992.09.22	14:05:56	36.294 (EHB)	52.722 (EHB)	5.1 (EHB)	35 (EHB)	268	44	75	GCMT
10	2008.03.26	18:49:54	36.349	52.697	4.6	38.5	9	74	159	(IIEES. Ya)
11	2012.03.18	2:38:15	36.33	52.78	4.3	10	13	84	166	IRSC
12	2012.01.11	17:08:02	36.489 (IIEES. Ya)	52.853 (IIEES. Ya)	5 (IIEES. Ya)	17.5 (IIEES. Ya)	114	31	71	GCMT
13	2018.09.22	22:34:44	36.65	52.98	4.4	15.6	144	20	76	IRSC
14	2000.08.16	12:53:02	36.706 (EHB)	54.366 (EHB)	4.9 (EHB)	25 (EHB)	240	34	78	GCMT
15	2004.10.07	21:46:15	37.1095576	54.4616255	4.7	22	27	46	53	GCMT
16	1985.10.29	14:23:05	36.901 (EHB)	54.899 (EHB)	6.2 (EHB)	13 (EHB)	113	21	124	ISC
17	1999.11.26	4:27:23	36.953 (EHB)	54.896 (EHB)	5.3 (EHB)	10 (EHB)	106	22	58	GCMT
18	2020.09.06	21:34:23	36.94	55.13	5	7	36	61	−7	IRSC
19	2018.08.16	6:41:49	36.82	55.22	4.4	6.5	253	64	16	IRSC
20	2014.06.13	9:12:27	36.857	55.081	4.3	8	80	43	122	IRSC
21	2011.08.11	22:32:16	36.592 (IIEES. Ya)	54.802 (IIEES. Ya)	5.2 (IIEES. Ya)	15.5 (IIEES. Ya)	97	43	77	GCMT
22	1985.10.29	13:13:41	36.68 (EHB)	54.772 (EHB)	6.1 (EHB)	15 (EHB)	97	31	122	GCMT
23	2014.09.06	21:34:19	36.67	54.76	4.4	10	164	27	119	IRSC
24	2006.12.20	5:00:36	36.072	53.855	4.3	20.5	257	71	165	(IIEES. Ya)
25	2013.03.21	19:37:03	36.142 (IRSC)	53.694 (IRSC)	4.6 (IRSC)	5 (IRSC)	78	73	3	GCMT
26	2012.04.22	6:38:56	35.947	53.374	4.2	13.5	206	73	−169	(IIEES. Ya)
27	2012.08.06	7:04:17	35.932	53.353	4.3	3.5	184	87	162	(IIEES. Ya)
28	2008.07.16	16:33:42	35.862	53.239	4.1	3.5	262	67	5	(IIEES. Ya)
29	1990.01.20	1:27:12	35.9 (EHB)	52.97 (EHB)	6 (EHB)	30 (EHB)	357	66	172	GCMT
30	2010.01.20	5:20:06	35.783	52.835	4.5	3.5	109	32	120	(IIEES. Ya)
31	2003.06.21	15:00:05	35.628 (EHB)	52.859 (EHB)	4.5 (EHB)	24 (EHB)	116	80	155	ZUR_RMT
32	2015.08.25	17:36:33	35.56	52.61	4.5	9	320	67	164	IRSC
33	1988.08.22	21:23:38	35.317 (EHB)	52.342 (EHB)	5.3 (EHB)	23 (EHB)	317	75	−175	GCMT
34	1988.08.23	5:30:51	35.377 (EHB)	52.246 (EHB)	5.2 (EHB)	25 (EHB)	348	32	−41	GCMT
35	2014.08.16	23:55:57	35.97	52.3	4.1	12	147	64	139	IRSC
36	1983.03.25	11:57:49	36.039 (EHB)	52.292 (EHB)	5.5 (EHB)	20 (EHB)	280	68	5	GCMT
37	1983.03.26	4:07:19	35.991 (EHB)	52.244 (EHB)	5.4 (EHB)	20 (EHB)	104	61	17	GCMT
38	2020.05.07	20:18:21	35.78 (IRSC)	52.05 (IRSC)	4.9 (IRSC)	7 (IRSC)	292	68	15	GCMT
39	2020.05.27	9:11:37	35.79	52.04	4	12	179	70	132	IRSC
40	2015.05.10	22:08:58	36.73	49.87	4.3	5	25	68	165	IRSC
41	1990.06.21	9:02:16	36.63 (EHB)	49.785 (EHB)	5.8 (EHB)	14 (EHB)	204	26	121	GCMT
42	2002.04.19	13:46:51	36.519 (EHB)	49.753 (EHB)	5.2 (EHB)	29 (EHB)	183	26	103	GCMT
43	1990.06.20	21:00:31	36.828 (EHB)	49.468 (EHB)	5.2 (EHB)	15 (EHB)	200	59	160	GCMT
44	1990.06.24	9:45:59	36.839 (EHB)	49.408 (EHB)	5.3 (EHB)	15 (EHB)	234	69	−163	GCMT
45	1990.07.06	19:34:52	36.864 (EHB)	49.298 (EHB)	5.3 (EHB)	20 (EHB)	94	37	6	GCMT
46	1991.11.28	17:19:56	36.827 (EHB)	49.584 (EHB)	5.6 (EHB)	15 (EHB)	219	36	130	GCMT
47	1995.10.15	6:56:35	37.03 (EHB)	49.473 (EHB)	5.2 (EHB)	25 (EHB)	66	49	178	GCMT
48	2002.02.14	20:06:22	36.933 (EHB)	49.46 (EHB)	4.2 (EHB)	15 (EHB)	61	81	−178	ZUR_RMT

which are subsidiary related to the principal fault planes (e.g., Lin et al., 2007; Chester et al., 1993). The pattern of antithetic and synthetic fractures and also oblique and dip- slip faults inside damage zones are related to (i) the growth process of the fault zone, (ii) the stress field variations during faulting, (iii) geometric controls, (iv) rock properties along the fault, (e.g., (Rashidi et al., 2022; Berg and Skar, 2005; Mandl, 2000). Many subsidiary faults were generated in the northern domain of Western and Central Alborz, and their geometry and kinematic characteristics depend on the North Alborz fault zone activities. Some of them have significant length introduced in this study and another study (e.g., Rashidi et al., 2021). The 60 km-long Royan and 30 km-long Kalardasht faults are two subsidiary faults dependent on the North Alborz fault zone activities with different mechanisms. The principal stress direction of the Alborz was generally estimated ~N035° (Rashidi and Derakhshani, 2022; Allen et al., 2003), which is compatible with the mechanism of the main fault planes and their subsidiary branches. In Fig. 13b, we specified faults with different strikes with different mechanisms in the compressive-shear zones related to the study region.

In the Western and Central Alborz, as seen in Fig. 13b, the faults have different mechanisms based on their strike related to the stress direction. System 1 (NE-SW) faults (parallel to the stress direction) appear as normal faults, system 2 (ENE–WSW) indicates both left-lateral strike-slip and dip-slip senses of shortening, systems 3 (NW–SE) show reverse and left-lateral strike-slip mechanism, systems 4 (N–S) are right- lateral strike-slip shear and reverse movements, system 5 (E-W) are left-lateral strike-slip shear (Fig. 13b). The strike-slip motions on each fault system in turn appears to correlate closely with synthetic and antithetic shears typical of a plane strain wrench tectonic regime in the region.

Each of these fault systems could have rotated due to the progressive collision of Central Iran with the South Caspian basin (after the middle-late Miocene; Mattei et al., 2017). This collision progressively wrapped the central and western parts of the Alborz mountains with clockwise rotations (Mattei et al., 2017). The current-day configuration and faults distributions with different mechanisms in the Alborz had been accompanied by a change in the stress direction from N-S to NE-SE in Pliocene (Ballato et al., 2013; Landgraf et al., 2009; Allen et al., 2003;

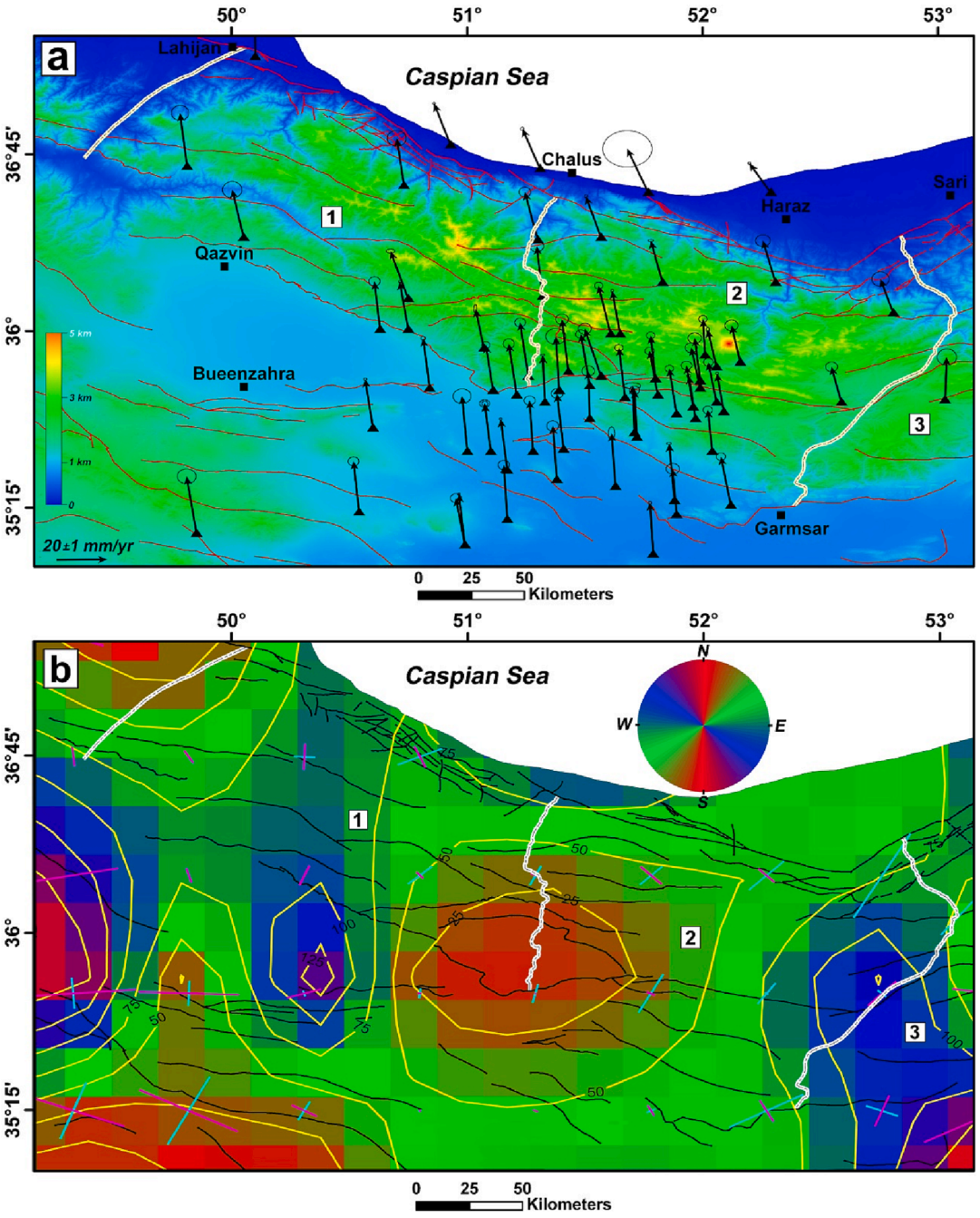

Fig. 12. GPS station velocities and geodetic strain map of the Western-Central Alborz and the surrounding region. (a) The GPS velocity vectors with their error ellipses. These are relative to the Eurasian reference frame. (b) The principal axes of the geodetic strain rate resulted from the GPS velocity vectors. Numbers 1, 2, and 3 are positions of the Western, Central, and Eastern Alborz, separated by white lines. The cyan and magenta color lines are the axes of the compressional and extensional strain rates, respectively. (For interpretation of the references to color in this figure legend, the reader is referred to the web version of this article.)

Jackson et al., 2002).

8. Conclusion

The analysis of the geometric and kinematic characteristics of active faults, seismicity, and geodetic data provides insight into the current-day kinematics of the Western and Central Alborz, which is crucial in understanding how the westward motion of the SCB with respect to Eurasia and Central Iran is accommodated in northern Iran. Our findings highlight the importance of the strain partitioning process in the Western and Central Alborz, which acts as a transpression zone with its northern and southern domains defined by the dominant NW-SE reverse faults such as the North Alborz fault zone and North Qazvin fault, respectively. The inner part of the transpression zone includes dominant WNW-ESE left-lateral strike-slip faults like the Rudbar and Mosha faults. The widening of the transpression zone upwards between inward-dipping walls aligns with the geometric features of the faults in the region.

Our field data of the northern domain of Western and Central Alborz delineates the North Alborz fault zone as an oblique fault zone including three active segments (the western, middle, and eastern segments) with some subsidiary fault branches (e.g., Royan, Kalardasht faults).

The western, middle, and eastern segments of the North Alborz fault zone include two, four, and three main fault planes, respectively. We, for

Table 2
GPS velocity vector data selected (from Khorrami et al. (2019)), their locations (Long. and Lat.), velocities (Evel and Nvel; mm/yr) and their uncertainties (SigVe and SigVn) with respect to Eurasia-fixed frame. R is the correlation coefficient between E and N velocities.

Site	Lon.	Lat.	Evel	Nvel	SigVe	SigVn	Cor	Solution
ABAL	51.986	35.793	−1.09	10.34	0.52	0.51	0.01	Raeesi
ABSD	52.0912	35.6612	−1.32	9.21	0.11	0.14	0.013	IPGN
AKHT	50.6006	35.5883	−1.52	11.71	0.13	0.1	0.014	IPGN
AMIN	52.586	35.701	−1.95	8.55	0.47	0.46	0.01	Raeesi
ARNG	51.0749	35.9284	−1.64	9.45	0.11	0.43	0.003	IPGN
ATTA	50.1	37.156	−0.14	13.5	2.1	2.09	0.03	Raeesi
BASH	53.025	35.705	0.32	10.28	0.76	0.78	0	Raeesi
BLDH	51.8287	36.2083	−2.3	10.03	0.21	0.11	0.015	IPGN
BOND	50.732	36.623	−1.37	11.28	0.74	0.76	0	Raeesi
BOOM	51.812	35.73	−1.62	10.61	0.36	0.34	0	Raeesi
CHIT	51.2132	35.7287	−1.55	12.31	0.44	0.47	0.002	IPGN
CHSH	50.988	35.088	−1.76	11.19	0.43	0.43	−0.001	Raeesi
CHSM	50.9894	35.0876	−1.2	12.13	0.1	0.09	0.019	IPGN
DAMA	52.059	35.701	−1.63	9.63	0.38	0.38	0.01	Raeesi
FOIM	51.166	35.4093	−1.29	12.25	0.11	0.11	0.014	IPGN
FOPM	50.84	35.7648	−1.26	11.93	0.2	0.17	0.005	IPGN
GARM	51.6457	35.985	−1.57	10.43	0.1	0.14	0.023	IPGN
GHAR	49.851	35.14	−1.92	13.59	0.74	0.72	−0.001	Raeesi
GHO1	49.812	36.699	−1.37	12.77	0.68	0.71	0	Raeesi
HELI	52.305	36.206	−2.47	10.03	0.58	0.56	0.02	Raeesi
HSGD	50.747	36.0067	−1.68	11.5	0.1	0.11	0.017	IPGN
LARZ	52.811	36.078	−2.49	8.2	0.68	0.69	0	Raeesi
MABD	52.2852	36.5884	−4.17	7.06	0.11	0.12	0.014	IPGN
MEHR	52.157	35.868	−1.71	8.88	0.52	0.52	0.01	Raeesi
MF01	51.955	35.683	−1.31	9.97	0.42	0.42	0	Raeesi
MF02	51.797	35.801	−0.96	10.39	0.33	0.33	0	Raeesi
MF03	51.885	35.649	−1.41	10.89	0.32	0.32	0	Raeesi
MF04	52.117	35.258	−1.94	11.65	0.36	0.36	0	Raeesi
MF05	51.277	35.493	−0.68	12.2	0.44	0.43	0	Raeesi
MF06	50.543	35.227	−1.07	12.17	0.43	0.43	−0.001	Raeesi
MF07	52.008	35.897	−0.4	8.74	0.33	0.34	0	Raeesi
MF10	51.304	36.394	−2.5	11.48	0.46	0.47	0	Raeesi
MF12	51.315	36.15	−1.12	12.04	0.54	0.54	0.01	Raeesi
MF13	50.632	36.009	−1.1	11.57	0.44	0.44	0	Raeesi
MF15	51.613	35.988	−2.37	11.65	0.33	0.33	−0.01	Raeesi
MF16	51.665	35.724	−1.17	11.92	0.33	0.33	0	Raeesi
MF17	51.108	35.753	−1.43	10.9	0.32	0.33	0	Raeesi
MOBK	51.7947	35.0529	−0.63	12.29	0.12	0.13	0.013	IPGN
NEYA	50.045	36.401	−2.21	11.43	0.76	0.8	0	Raeesi
NKAD	51.3098	36.685	−3.43	9.59	0.13	0.16	0.009	IPGN
NOSH	51.768	36.586	−4.08	10.47	1.93	1.75	0	Raeesi
PISH	51.885	35.224	−0.76	10.97	0.52	0.51	0.01	Raeesi
PLOR	52.064	35.8496	−1.72	8.93	0.11	0.27	0.007	IPGN
PLZI	51.971	35.6303	−1.31	10.25	0.15	0.18	0.006	IPGN
POOL	51.5742	36.4031	−2.97	9.91	0.13	0.16	0.009	IPGN
ROKM	51.0983	35.4872	−1.21	11.49	0.4	0.36	0.001	IPGN
RSHT	49.6244	37.323	−2.29	12.89	0.1	0.1	0.017	IPGN
RTCL	51.711	35.5744	−0.37	11.24	0.65	0.3	0	IPGN
RTKM	51.0989	35.4864	−1.17	11.46	0.22	0.26	0.004	IPGN
SHOR	51.8842	35.2772	−1.05	13.62	0.17	0.12	0.009	IPGN
TANG	52.043	35.492	−0.85	9.97	0.36	0.36	0.01	Raeesi
TEHN	51.3341	35.6973	−0.43	11.28	0.16	0.1	0.01	IPGN
TEHR	51.386	35.747	−0.65	12.94	0.79	0.75	0.01	Raeesi
TF01	51.257	35.812	−1.6	12.9	0.42	0.42	0.01	Raeesi
TF09	51.425	35.833	−1.25	12.56	0.5	0.5	0.01	Raeesi
TF16	51.522	35.774	−1.7	12.36	0.41	0.41	0.01	Raeesi
TF20	51.568	35.808	−3.19	11.43	0.51	0.52	0.01	Raeesi
TKBN	50.9301	36.7859	−3.22	9.94	0.1	0.11	0.015	IPGN
TLGN	50.745	36.1436	−3.43	11.42	0.34	0.18	0.002	IPGN
TN01	51	35.493	−1.03	13.22	0.7	0.7	0.02	Raeesi
TN02	51.17	35.203	−0.68	12.99	0.45	0.46	0.009	Raeesi
TN03	51.379	35.366	−0.78	12.85	0.48	0.49	0.01	Raeesi
TN04	51.409	35.495	−1.28	13.3	0.46	0.47	0.01	Raeesi
TN05	51.515	35.633	−0.31	11.41	0.49	0.5	0.01	Raeesi
TN06	51.724	35.55	−0.46	11.3	0.4	0.4	0.01	Raeesi
TN07	51.994	35.763	−1.75	9.72	0.47	0.48	0.01	Raeesi
VRMN	51.632	35.344	−0.77	12.72	0.25	0.63	0	Raeesi

the first time, specify the structural characteristics of all planes related to the middle and eastern segments, which can be used as basic data in seismic hazard assessment. In seismic hazard assessment, each of these planes must be considered as a potential source of destructive earthquakes.

The main fault planes related to each segment commonly have reverse mechanisms and left-lateral strike-slip components. We determine 5 main systems of fault kinematics along the 300 km North Alborz fault zone, which justifies the different mechanisms of active subsidiary faults with significant length in the northern domain of the zone.

Table 3
Geodetic strain rate axes trend and magnitude at grid nodes with 0.2-degree spacing. Long. and Lat. are the locations of GPS stations, respectively and $\dot{\epsilon}_{max}$ is the magnitude of the compressional strain rate.

No.	lon	lat	Trend	$\dot{\epsilon}_{max}$
1	49.25	34.25	135.441	3.3224
2	49.75	34.25	135.4408	0.43254
3	49.75	34.25	62.2839	1.36366
4	49.25	34.75	62.284	1.17677
5	49.75	34.75	152.284	2.77391
6	50.25	34.25	152.2839	0.250557
7	50.25	34.25	31.587	0.939554
8	50.75	34.25	31.5867	0.43124
9	50.25	34.75	39.143	1.73541
10	50.75	34.75	39.143	0.936281
11	51.25	34.75	171.71	0.165433
12	52.25	34.25	171.71	1.22221
13	52.75	34.25	81.71	3.73E-002
14	52.75	34.25	81.7095	2.02105
15	52.25	34.75	78.026	1.21909
16	52.75	34.75	78.0263	6.21E-002
17	52.75	34.75	51.38	0.978687
18	53.25	34.25	51.3801	0.165382
19	53.25	34.25	71.08	0.568246
20	53.75	34.25	71.0804	0.862947
21	53.25	34.75	72.462	0.662288
22	49.25	35.25	72.4618	1.50543
23	49.75	35.25	94.6072	1.91616
24	49.25	35.75	94.6072	0.770751
25	49.75	35.75	24.2696	0.627337
26	50.25	35.25	24.27	0.515908
27	50.75	35.25	114.27	6.94E-002
28	50.25	35.75	114.2696	0.145212
29	50.75	35.75	73.085	0.24689
30	51.75	35.25	73.0849	0.195652
31	51.25	35.75	158.57	0.473526
32	51.75	35.75	158.57	1.08765
33	52.25	35.25	68.57	1.73789
34	52.75	35.25	68.5702	0.698537
35	52.25	35.75	22.6738	7.67E-002
36	52.25	35.75	22.674	0.633548
37	52.75	35.75	112.674	0.234915
38	53.25	35.25	112.6738	1.18161
39	53.75	35.25	58.471	1.22648
40	53.25	35.75	58.4713	0.736697
41	53.75	35.75	146.09	1.05639
42	50.75	36.25	146.0903	0.657595
43	50.25	36.75	20.763	0.429469
44	50.75	36.75	20.7628	0.999157
45	51.25	36.25	27.196	0.53494
46	51.75	36.25	27.1955	0.653147
47	51.25	36.75	175.557	6.00E-002
48	51.75	36.75	175.55737	5.88E-002
49	52.25	36.25	2.039	1.01838
50	52.75	36.25	2.03879	0.211563
51	52.75	36.25	28.199	2.40157
52	52.25	36.75	28.199	1.17484
53	52.75	36.75	59.395	2.16855
54	53.25	36.25	59.3952	0.31947
55	53.25	36.25	162.706	3.77777
56	53.75	36.25	162.7057	1.39846
57	53.75	36.25	6.782	3.16122
58	53.25	36.75	6.78169	1.04497
59	53.25	36.75	63.204	2.34839
60	53.75	36.75	63.2043	4.54366
61	49.25	37.25	13.494	0.158218
62	49.75	37.25	13.4938	0.167688
63	49.25	37.75	27.945	0.623877
64	49.75	37.75	27.9447	0.376631
65	50.25	37.25	61.839	0.601409
66	50.75	37.25	61.8389	0.826765
67	50.25	37.75	111.062	0.602614
68	52.25	37.25	111.0623	0.505112
69	52.75	37.25	125.611	1.00221
70	52.75	37.75	125.611	7.05E-002
71	53.25	37.25	35.611	2.95E-002
72	53.75	37.25	35.6113	1.79258
73	53.75	37.75	133.838	1.19574

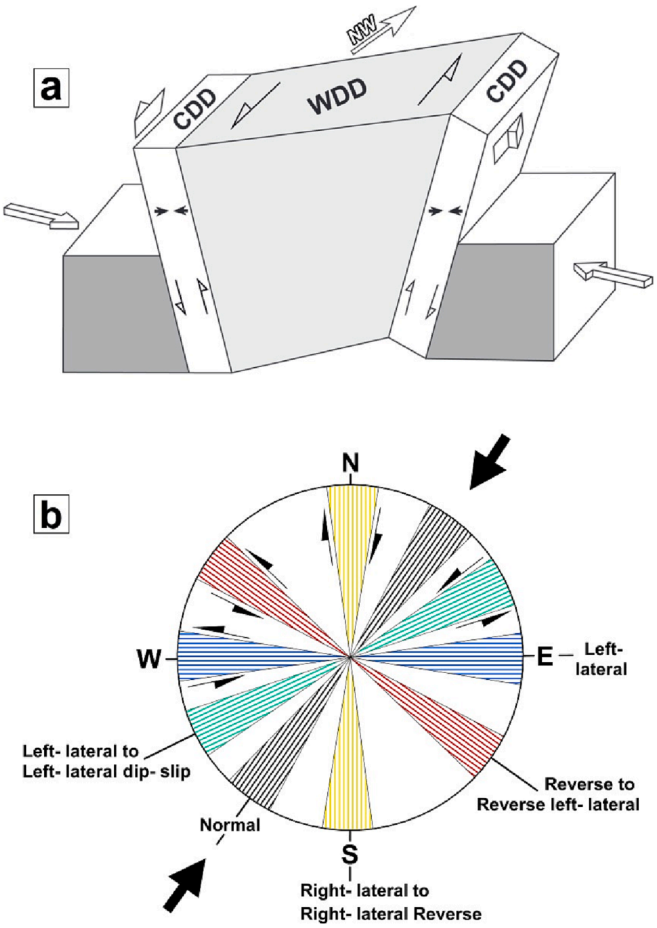

Fig. 13. Proposed tectonic evolution model for the active faults in the Western and Central Alborz and their northern domains. (a) The left-lateral trans-pression model with widening upwards between inward-dipping walls where strain is partitioned into inner-domain wrench dominated (WDD) and contraction dominated (CDD) domains. (b) A schematic kinematic model of the active faults in the northern domain of Western and Central Alborz.

High seismic activity is observed in areas with higher magnitudes of compressional geodetic strain rate principal axes, which confirms the mechanism of movement of the North Alborz fault planes. Geodetic calculations reveal anomalies in the strain rate of the Western-Central Alborz and its surrounding regions. The anomaly within the 25-degree contour in the southern domain of the Alborz is associated with the North Tehran fault and represents the reverse mechanism of movement. The anomaly within the 125-degree contour to the west is interpreted as the effect of the Eshtehard fault, and the anomaly within the 100-degree contour line to the east is located on the Semnan and Garmsar faults.

Declaration of Competing Interest

The authors declare that they have no known competing financial interests or personal relationships that could have appeared to influence the work reported in this paper.

Data availability

No data was used for the research described in the article.

Acknowledgments

We thank the editor Michel Faure and the reviewer Paolo Ballato and anonymous reviewer for useful comments on the manuscript. This study

is the result of a collaborative research effort involving Shahid Bahonar University of Kerman (SBUK) in Kerman, Iran; the International Institute of Earthquake Engineering and Seismology (IIEES) in Tehran, Iran; Utrecht University in the Netherlands; and the University of Trieste in Trieste, Italy. We would like to express our gratitude for the logistical support provided by SBUK and support by the project MIUR-PRIN 2017.

References

Abbassi, A., Nasrabadi, A., Tatar, M., Yaminifard, F., Abbassi, M.R., Hatzfeld, D., Priestley, K., 2010. Crustal velocity structure in the southern edge of the Central Alborz (Iran). J. Geodyn. 49 (2), 68–78. https://doi.org/10.1016/j.jog.2009.09.044.

Abbassi, M., Hatzfeld, D., Kamalian, N., 2005. Microseismicity in the region of Tehran. Tectonophysics 395 (3–4), 193–208. https://doi.org/10.1016/j.tecto.2004.09.011.

Akasheh, B., Berckhemer, H., 1984. Focal mechanism of earthquakes in Iran with special emphasis on small shocks in the tehran region. Neues Jahrbuch Für Geologie Und Paläontologie - Abhandlungen 168 (2–3), 244–255. https://doi.org/10.1127/njgpa/168/1984/244.

Allen, M., Ghassemi, M.R., Shahrabi, M., Qorashi, M., 2003. Accommodation of late Cenozoic oblique shortening in the Alborz range, northern Iran. J. Struct. Geol. 25 (5), 659–672. https://doi.org/10.1016/S0191-8141(02)00064-0.

Allen, M., Jackson, J., Walker, R., 2004. Late Cenozoic reorganization of the Arabia-Eurasia collision and the comparison of short-term and long-term deformation rates: Arabia-Eurasia collision. Tectonics 23 (2), n/a-n/a. https://doi.org/10.1029/2003TC001530.

Allmendinger, R., 2001. Fault Kin Win [English].

Ambraseys, N.N., Melville, C.A., 1982. A History of Persian Earthquakes. Cambridge University Press, London, UK.

Ambraseys, N.N., Moinfar, A.A., 2010. The sessmicity of IRAN: the Torud earthquake of 12th february 1953. Ann. Geophys. 30 (1–2) https://doi.org/10.4401/ag-4817.

Ballato, P., Landgraf, A., Schildgen, T.F., Stockli, D.F., Fox, M., Ghassemi, M.R., Kirby, E., Strecker, M.R., 2015. The growth of a mountain belt forced by base-level fall: tectonics and surface processes during the evolution of the Alborz Mountains, N Iran. Earth Planet. Sci. Lett. 425, 204–218. https://doi.org/10.1016/j.epsl.2015.05.051.

Ballato, P., Stockli, D.F., Ghassemi, M.R., Landgraf, A., Strecker, M.R., Hassanzadeh, J., Friedrich, A., Tabatabaei, S.H., 2013. Accommodation of transpressional strain in the Arabia-Eurasia collision zone: new constraints from (U-Th)/He thermochronology in the Alborz mountains, north Iran: COLLISIONAL OBLIQUE STRAIN. Tectonics 32 (1), 1–18. https://doi.org/10.1029/2012TC003159.

Ballato, P., Uba, C.E., Landgraf, A., Strecker, M.R., Sudo, M., Stockli, D.F., Friedrich, A., Tabatabaei, S.H., 2011. Arabia-Eurasia continental collision: insights from late Tertiary foreland-basin evolution in the Alborz Mountains, northern Iran. Geol. Soc. Am. Bull. 123 (1–2), 106–131. https://doi.org/10.1130/B30091.1.

Barbot, S., Luo, H., Wang, T., Hamiel, Y., Piatibratova, O., Javed, M.T., Braitenberg, C., Gurbuz, G., 2023. Slip distribution of the February 6, 2023 Mw 7.8 and Mw 7.6, Kahramanmaraş, Turkey earthquake sequence in the East Anatolian Fault Zone. Seismica 2 (3). https://doi.org/10.26443/seismica.v2i3.502.

Beavan, J., Haines, J., 2001. Contemporary horizontal velocity and strain rate fields of the Pacific-Australian plate boundary zone through New Zealand. J. Geophys. Res. Solid Earth 106 (B1), 741–770. https://doi.org/10.1029/2000JB900302.

Berberian, F., Berberian, M., 1981. Tectono-plutonic episodes in Iran. In: Gupta, H.K., Delany, F.M. (Eds.), Geodynamics Series, vol. 3. American Geophysical Union, pp. 5–32. https://doi.org/10.1029/GD003p0005.

Berberian, M., 1983. The southern Caspian: a compressional depression floored by a trapped, modified oceanic crust“. Can. J. Earth Sci. 20 (2), 163–183. https://doi.org/10.1139/e83-015.

Berberian, M., 1997. Seismic sources of the transcaucasian historical earthquakes. In: Giardini, D., Balassanian, S. (Eds.), Historical and Prehistorical Earthquakes in the Caucasus. Springer, Netherlands, pp. 233–311. https://doi.org/10.1007/978-94-011-5464-2_13.

Berberian, M., King, G.C.P., 1981. Towards a paleogeography and tectonic evolution of Iran. Can. J. Earth Sci. 18 (2), 210–265. https://doi.org/10.1139/e81-019.

Berberian, M., Qorashi, M., Jackson, J.A., Priestley, K., Wallace, T., 1992. The Rudbar-Tarom earthquake of June 20, 1990 in NW Persia: Preliminary field and seismological observations, and its tectonic significance. 82, 1726–1755.

Berberian, M., Walker, R., 2010. The Rudbār Mw 7.3 earthquake of 1990 June 20; seismotectonics, coseismic and geomorphic displacements, and historic earthquakes of the western ‘High-Alborz’, Iran: the Rudbār Mw 7.3 earthquake of 1990 June 20. Geophys. J. Int. 182(3), 1577–1602. https://doi.org/10.1111/j.1365-246X.2010.04705.x.

Berberian, M., Yeats, R.S., 1999. Patterns of historical rupture in the Iranian Plateau. Bull. Seismol. Soc. Am. 89 (1), 120–139.

Berberian, M., Yeats, R.S., 2001. Contribution of archaeological data to studies of earthquake history in the Iranian Plateau. J. Struct. Geol. 23 (2–3), 563–584. https://doi.org/10.1016/S0191-8141(00)00115-2.

Berg, S.S., Skar, T., 2005. Controls on damage zone asymmetry of a normal fault zone: Outcrop analyses of a segment of the Moab fault, SE Utah. J. Struct. Geol. 27 (10), 1803–1822. https://doi.org/10.1016/j.jsg.2005.04.012.

Brunet, M.F., Korotaev, M.V., Ershov, A.V., Nikishin, A.M., 2003. The South Caspian Basin: a review of its evolution from subsidence modelling. Sed. Geol. 156 (1–4), 119–148. https://doi.org/10.1016/S0037-0738(02)00285-3.

Casas, A.M., Gapais, D., Nalpas, T., Besnard, K., Román-Berdiel, T., 2001. Analogue models of transpressive systems. J. Struct. Geol. 23 (5), 733–743. https://doi.org/10.1016/S0191-8141(00)00153-X.

Chen, R.F., Lin, C.W., Chen, Y.H., He, T.C., Fei, L.Y., 2015. Detecting and characterizing active thrust fault and deep-seated landslides in dense forest areas of southern taiwan using airborne LiDAR DEM. Remote Sens. (Basel) 7 (11), 15443–15466. https://doi.org/10.3390/rs71115443.

Chester, F.M., Evans, J.P., Biegel, R.L., 1993. Internal structure and weakening mechanisms of the San Andreas Fault. J. Geophys. Res. Solid Earth 98 (B1), 771–786. https://doi.org/10.1029/92JB01866.

Cowie, P.A., Scholz, C.H., 1992. Physical explanation for the displacement-length relationship of faults using a post-yield fracture mechanics model. J. Struct. Geol. 14 (10), 1133–1148. https://doi.org/10.1016/0191-8141(92)90065-5.

Davoudzadeh, M., Weber-Diefenbach, K., 1997. Paleogeography, stratigraphy, and tectonics of the tertiary of Iran. Neues Jahrbuch Für Geologie Und Paläontologie - Abhandlungen 205 (1), 33–67. https://doi.org/10.1127/njgpa/205/1997/33.

Dayal, P., 2010. A Text Book of Geomorphology. Rajesh Publications.

De Pascale, G.P., Chandler-Yates, N., Dela Pena, F., Wilson, P., May, E., Twiss, A., Cheng, C., 2016. Active tectonics west of New Zealand’s alpine fault: South Westland fault zone activity shows australian plate instability. Geophys. Res. Lett. 43 (7), 3120–3125. https://doi.org/10.1002/2016GL068233.

Derakhshani, R., Zaresefat, M., Nikpeyman, V., GhasemiNejad, A., Shafieibafti, S., Rashidi, A., Nemati, M., Raoof, A., 2023. Machine learning-based assessment of watershed morphometry in makran. Land 12 (4), 776. https://doi.org/10.3390/land12040776.

Dewey, J.F., Holdsworth, R.E., Strachan, R.A., 1998. Transpression and transtension zones. Geol. Soc. Lond. Spec. Publ. 135 (1), 1–14. https://doi.org/10.1144/GSL.SP.1998.135.01.01.

Djamour, Y., Vernant, P., Bayer, R., Nankali, H.R., Ritz, J.F., Hinderer, J., Hatam, Y., Luck, B., Le Moigne, N., Sedighi, M., Khorrami, F., 2010. GPS and gravity constraints on continental deformation in the Alborz mountain range, Iran: GPS and gravity measurements in Alborz. Geophys. J. Int. 183 (3), 1287–1301. https://doi.org/10.1111/j.1365-246X.2010.04811.x.

Donner, S., Rößler, D., Krüger, F., Ghods, A., Strecker, M.R., 2013. Segmented seismicity of the M w 6.2 Baladeh earthquake sequence (Alborz Mountains, Iran) revealed from regional moment tensors. J. Seismol. 17 (3), 925–959. https://doi.org/10.1007/s10950-013-9362-7.

Engdahl, R., Jackson, J.A., Myers, S.C., Bergman, E.A., Priestley, K., 2006. Relocation and assessment of seismicity in the Iran region. Geophys. J. Int. 167 (2), 761–778. https://doi.org/10.1111/j.1365-246X.2006.03127.x.

Ezati, M., Gholami, E., Mousavi, S.M., Rashidi, A., Derakhshani, R., 2022. Active deformation patterns in the northern birjand mountains of the sistan suture zone, Iran. Appl. Sci. 12 (13), 6625. https://doi.org/10.3390/app12136625.

Ghassemi, M. R., 1990. Geology, stratigraphy, and structural geology of Chahardeh area, eastern Alborz [MSc]. Tehran.

Ghassemi, M.R., 2005. Drainage evolution in response to fold growth in the hanging-wall of the Khazar fault, north-eastern Alborz, Iran. Basin Res. 17 (3), 425–436. https://doi.org/10.1111/j.1365-2117.2005.00271.x.

Ghassemi, M.R., Fattahi, M., Landgraf, A., Ahmadi, M., Ballato, P., Tabatabaei, S.H., 2014. Kinematic links between the Eastern Mosha Fault and the North Tehran Fault, Alborz range, northern Iran. Tectonophysics 622, 81–95. https://doi.org/10.1016/j.tecto.2014.03.007.

Goswami, P.K., Pant, C.C., Pandey, S., 2009. Tectonic controls on the geomorphic evolution of alluvial fans in the Piedmont Zone of Ganga Plain, Uttarakhand, India. J. Earth Syst. Sci. 118 (3), 245–259. https://doi.org/10.1007/s12040-009-0012-y.

Harland, W.B., 1971. Tectonic transpression in Caledonian Spitsbergen. Geol. Mag. 108 (1), 27–41. https://doi.org/10.1017/S0016756800050937.

Hessami, K., 2017. Seismotectonics in the Golestan province (Research Internal; p. 81). International Institute of Earthquake Engineering and Seismology.

Hessami, K., Mobayyen, F., Tabassi, H., 2013. Active fault map of Iran [Map]. International institute of earthquake engineering and seismology.

Hoffman, P.F., 1987. Continental transform tectonics: Great Slave Lake shear zone (ca. 1.9 Ga), northwest Canada. Geology, 15(9), 785. <https://doi.org/10.1130/0091-7613(1987)15<785:CTTGSL>2.0.CO;2>.

Hollingsworth, J., Jackson, J., Walker, R., Nazari, H., 2008. Extrusion tectonics and subduction in the eastern South Caspian region since 10 Ma. Geology 36 (10), 763. https://doi.org/10.1130/G25008A.1.

Holt, W.E., Li, M., Haines, A.J., 1995. Earthquake strain rates and instantaneous relative motions within central and eastern Asia. Geophys. J. Int. 122 (2), 569–593. https://doi.org/10.1111/j.1365-246X.1995.tb07014.x.

Huber, H., & Eftekhar-Nezhad, J. (1978a). Geological map of Iran, sheet no. 1, northwest Iran [Map]. National Iranian Oil Company.

Huber, H., Eftekhar-Nezhad, J., 1978b. Geological map of Iran, sheet no. 2, north-central Iran [Map]. National Iranian Oil Company.

Jackson, J., Haines, J., Holt, W., 1995. The accommodation of Arabia-Eurasia Plate convergence in Iran. J. Geophys. Res. Solid Earth 100 (B8), 15205–15219. https://doi.org/10.1029/95JB01294.

Jackson, J., Priestley, K., Allen, M., Berberian, M., 2002. Active tectonics of the South Caspian Basin. Geophys. J. Int. 148 (2), 214–245. https://doi.org/10.1046/j.1365-246X.2002.01588.x.

Javidfakhr, B., Bellier, O., Shabanian, E., Ahmadian, S., Saidi, A., 2011. Plio-Quaternary tectonic regime changes in the transition zone between Alborz and Kopeh Dagh mountain ranges (NE Iran). Tectonophysics 506 (1–4), 86–108. https://doi.org/10.1016/j.tecto.2011.04.013.

Jones, R.R., Holdsworth, R.E., Clegg, P., McCaffrey, K., Tavarnelli, E., 2004. Inclined transpression. J. Struct. Geol. 26 (8), 1531–1548. https://doi.org/10.1016/j.jsg.2004.01.004.

Kadinsky-Cade, K., Barazangi, M., Oliver, J., Isacks, B., 1981. Lateral variations of high-frequency seismic wave propagation at regional distances across the Turkish and Iranian plateaus. J. Geophys. Res. Solid Earth 86 (B10), 9377–9396. https://doi.org/10.1029/JB086iB10p09377.

Keiding, M., Kreemer, C., Lindholm, C.D., Abbasi, S., Olesen, O., Kierulf, H.P., 2015. A comparison of strain rates and seismicity for Fennoscandia: depth dependency of deformation from glacial isostatic adjustment. Geophys. J. Int. 202 (2), 1021–1028. https://doi.org/10.1093/gji/ggv207.

Keller, E. A., Pinter, N., 2002. Active Tectonics: Earthquakes, Uplift, and Landscape.

Khin, K., Moe, A., Myint, M., Aung, K.P., 2021. Dextral transpressional shearing and strike-slip partitioning developments in the Central Myanmar Basin during the collision between the India Plate and West Myanmar Block. J. Asian Earth Sci.: X 5, 100055. https://doi.org/10.1016/j.jaesx.2021.100055.

Khorrami, F., Vernant, P., Masson, F., Nilfouroushan, F., Mousavi, Z., Nankali, H., Saadat, S.A., Walpersdorf, A., Hosseini, S., Tavakoli, P., Aghamohammadi, A., Alijanzade, M., 2019. An up-to-date crustal deformation map of Iran using integrated campaign-mode and permanent GPS velocities. Geophys. J. Int. 217 (2), 832–843. https://doi.org/10.1093/gji/ggz045.

Kosarev, A. N., Kostiany, G., 2010. The Caspian Sea Encyclopaedia.

Landgraf, A., Ballato, P., Strecker, M.R., Friedrich, A., Tabatabaei, S.H., Shahpasandzadeh, M., 2009. Fault-kinematic and geomorphic observations along the North Tehran Thrust and Mosha Fasham Fault, Alborz mountains Iran: Implications for fault-system evolution and interaction in a changing tectonic regime. Geophys. J. Int. 177 (2), 676–690. https://doi.org/10.1111/j.1365-246X.2009.04089.x.

Lin, A., Maruyama, T., Kobayashi, K., 2007. Tectonic implications of damage zone-related fault-fracture networks revealed in drill core through the Nojima fault, Japan. Tectonophysics 443 (3–4), 161–173. https://doi.org/10.1016/j.tecto.2007.01.011.

Mandl, G., 2000. Faulting in Brittle Rocks. In Introduction to the Mechanics of Tectonics. Springer.

Mangino, S., Priestley, K., 1998. The crustal structure of the southern Caspian region. Geophys. J. Int. 133 (3), 630–648. https://doi.org/10.1046/j.1365-246X.1998.00520.x.

Masson, F., Chéry, J., Hatzfeld, D., Martinod, J., Vernant, P., Tavakoli, F., Ghafory-Ashtiani, M., 2004. Seismic versus aseismic deformation in Iran inferred from earthquakes and geodetic data: Seismic versus aseismic deformation in Iran. Geophys. J. Int. 160 (1), 217–226. https://doi.org/10.1111/j.1365-246X.2004.02465.x.

Mattei, M., Cifelli, F., Alimohammadian, H., Rashid, H., Winkler, A., Sagnotti, L., 2017. Oroclinal bending in the Alborz Mountains (Northern Iran): New constraints on the age of South Caspian subduction and extrusion tectonics. Gondw. Res. 42, 13–28. https://doi.org/10.1016/j.gr.2016.10.003.

McQuarrie, N., Van Hinsbergen, D., 2013. Retrodeforming the Arabia-Eurasia collision zone: age of collision versus magnitude of continental subduction. Geology 41 (3), 315–318. https://doi.org/10.1130/G33591.1.

Mehrabi, A., Pirasteh, S., Rashidi, A., Pourkhosravani, M., Derakhshani, R., Liu, G., Mao, W., Xiang, W., 2021. Incorporating persistent scatterer interferometry and radon anomaly to understand the anar fault mechanism and observing new evidence of intensified activity. Remote Sens. (Basel) 13 (11), 2072. https://doi.org/10.3390/rs13112072.

Mohammadi Nia, A., Rashidi, A., Khatib, M.M., Mousavi, S.M., Nemati, M., Shafieibafti, S., Derakhshani, R., 2023. Seismic risk in alborz: insights from geological moment rate estimation and fault activity analysis. Appl. Sci. 13 (10), 6236. https://doi.org/10.3390/app13106236.

Motaghi, K., Ghods, A., Sobouti, F., Shabanian, E., Mahmoudabadi, M., Priestley, K., 2018. Lithospheric seismic structure of the West Alborz – Talesh ranges, Iran. Geophys. J. Int. 215 (3), 1766–1780. https://doi.org/10.1093/gji/ggy372.

Mouthereau, F., Lacombe, O., Vergés, J., 2012. Building the Zagros collisional orogen: timing, strain distribution and the dynamics of Arabia/Eurasia plate convergence. Tectonophysics 532–535, 27–60. https://doi.org/10.1016/j.tecto.2012.01.022.

Mukherjee, S., Koyi, H.A., 2010. Higher Himalayan Shear Zone, Sutlej section: Structural geology and extrusion mechanism by various combinations of simple shear, pure shear and channel flow in shifting modes. Int. J. Earth Sci. 99 (6), 1267–1303. https://doi.org/10.1007/s00531-009-0459-8.

Nabavi, M.H., 1976. An INTRODUCTION to the geology of Iran. Geological Survey of Iran.

Nabavi, S.T., Díaz-Azpiroz, M., Talbot, C.J., 2017. Inclined transpression in the Neka Valley, eastern Alborz, Iran. Int. J. Earth Sci. 106 (5), 1815–1840. https://doi.org/10.1007/s00531-016-1388-y.

Nazari, H., 2006. Analyse de la tectonique recente et active dans l'Alborz Central et la region de Teheran: Approche morphotectonique et paleoseismologique [PhD]. Montpellier II.

Nazari, H., Ritz, J.F., 2008. Neotectonics in Central Alborz. Geosci. Geol. Surv. Iran 17, 74–92.

Nazari, H., Ritz, J.F., Burg, J.P., Shokri, M., Haghipour, N., Mohammadi Vizheh, M., Avagyan, A., Fazeli Nashli, H., Ensani, M.R., 2021. Active tectonics along the Khazar fault (Alborz, Iran). J. Asian Earth Sci. 219, 104893 https://doi.org/10.1016/j.jseaes.2021.104893.

Nazari, H., Ritz, J.-F., Salamati, R., Shafei, A., Ghassemi, A., Michelot, J.-L., Massault, M., Ghorashi, M., 2009. Morphological and palaeoseismological analysis along the Taleghan fault (Central Alborz, Iran). Geophys. J. Int. 178 (2), 1028–1041. https://doi.org/10.1111/j.1365-246X.2009.04173.x.

Nazari, H., Ritz, J.-F., Walker, R.T., Salamati, R., Rizza, M., Patnaik, R., Hollingsworth, J., Alimohammadian, H., Jalali, A., Kaveh Firouz, A., Shahidi, A., 2014. Palaeoseismic evidence for a medieval earthquake, and preliminary estimate of late Pleistocene slip-rate, on the Firouzkuh strike-slip fault in the Central Alborz region of Iran. J. Asian Earth Sci. 82, 124–135. https://doi.org/10.1016/j.jseaes.2013.12.018.

Nemati, M., 2015. Insights into the aftershocks and inter-seismicity of some large Persian earthquakes. 26 (1), 35–48.

Nemati, M., Hatzfeld, D., Gheitanchi, M.R., Sadidkhouy, A., Mirzaei, N., 2011. Microseismicity and seismotectonics of the Firuzkuh and Astaneh faults (East Alborz, Iran). Tectonophysics 506 (1–4), 11–21. https://doi.org/10.1016/j.tecto.2011.04.007.

Nemati, M., Hatzfeld, D., Gheitanchi, M., Sadidkhouy, A., Mirzaei, N., 2012. Detailed crustal discontinuities, seismotectonic and seismicity parameters of the east Alborz, Iran, is flower structure as subsurface fault geometry? Inst. Geophys. Univ. Tehran 38 (2), 1–15.

Pourbeyranvand, S., 2021. Stress mapping focal mechanism display and stress tensor inversion in Qeshm Island southern Iran. Iran. J. Geophys., Online First. https://doi.org/10.30499/ijg.2021.260899.1307.

Priestley, K., Baker, C., Jackson, J., 1994. Implications of earthquake focal mechanism data for the active tectonics of the south Caspian Basin and surrounding regions. Geophys. J. Int. 118 (1), 111–141. https://doi.org/10.1111/j.1365-246X.1994.tb04679.x.

Raeesi, M., Zarifi, Z., Nilfouroushan, F., Boroujeni, S.A., Tiampo, K., 2017. Quantitative analysis of seismicity in Iran. Pure Appl. Geophys. 174 (3), 793–833. https://doi.org/10.1007/s00024-016-1435-4.

Rahnama, J., Derakhshan, R., Alsop, G.I., Ghorbani, H., 2008. Basement faults and salt plug emplacement in the arabian platform in southern Iran. J. Appl. Sci. 8 (18), 3235–3241. https://doi.org/10.3923/jas.2008.3235.3241.

Rashidi, A., 2021. Geometric and kinematic characteristics of the Khazar and North Alborz Faults: Links to the structural evolution of the North Alborz-South Caspian boundary, Northern Iran. J. Asian Earth Sci. 213, 104755 https://doi.org/10.1016/j.jseaes.2021.104755.

Rashidi, A., Derakhshani, R., 2022. Strain and moment rates from GPS and seismological data in Northern Iran: implications for an evaluation of stress trajectories and probabilistic fault rupture hazard. Remote Sens. (Basel) 14 (9), 2219. https://doi.org/10.3390/rs14092219.

Rashidi, A., Khatib, M.M., Derakhshani, R., 2022a. Structural characteristics and formation mechanism of the earth fissures as a geohazard in Birjand. IranAppl. Sci. 12 (9), 4144. https://doi.org/10.3390/app12094144.

Rashidi, A., Kianimehr, H., Shafieibafti, S., Mehrabi, A., Derakhshani, R., 2021. Active faults in the west of the Lut block (central Iran). Geophys. Res. 22 (3), 70–84. https://doi.org/10.21455/gr2021.3-5.

Rashidi, A., Kianimehr, H., Yamini-Fard, F., Tatar, M., Zafarani, H., 2022b. Present stress map and deformation distribution in the NE lut block, Eastern Iran: insights from seismic and geodetic strain and moment rates. Pure Appl. Geophys. 179 (5), 1887–1917. https://doi.org/10.1007/s00024-022-03015-x.

Rashidi, A., Shafieibafti, S., Nemati, M., Ezati, M., Gholami, E., Mousavi, S.M., Derakhshani, R., 2023. Flexural-slip folding in buckling phases of orogenic belts: Insight into the tectonic evolution of fault splays in the East Iran orogen. Front. Earth Sci. 11, 1169667. https://doi.org/10.3389/feart.2023.1169667.

Rashidi, A., Shahpasandzadeh, M., Braitenberg, C., 2022c. Late cenozoic to present kinematic of the north to eastern iran orogen: accommodating opposite sense of fault blocks rotation. Remote Sens. (Basel) 14 (16), 4048. https://doi.org/10.3390/rs14164048.

Rezapour, M., 1991. Study of Mechanism & Aftershocks of 1990 Roudbar-Manjil earthquake [M.Sc]. Geophysics Institute, University of Tehran.

Ritz, J.F., Nazari, H., Balescu, S., Lamothe, M., Salamati, R., Ghassemi, A., Shafei, A., Ghorashi, M., Saidi, A., 2012. Paleoearthquakes of the past 30,000 years along the North Tehran Fault (Iran): PALEOSEISMOLOGY OF NORTH TEHRAN FAULT. J. Geophys. Res.: Solid Earth 117 (B6), n/a-n/a. https://doi.org/10.1029/2012JB009147.

Ritz, J.-F., Nazari, H., Ghassemi, A., Salamati, R., Shafei, A., Solaymani, S., Vernant, P., 2006. Active transtension inside central Alborz: a new insight into northern Iran–southern Caspian geodynamics. Geology 34 (6), 477. https://doi.org/10.1130/G22319.1.

Rizza, M., Mahan, S., Ritz, J.-F., Nazari, H., Hollingsworth, J., Salamati, R., 2011. Using luminescence dating of coarse matrix material to estimate the slip rate of the Astaneh fault, Iran. Quat. Geochronol. 6 (3–4), 390–406. https://doi.org/10.1016/j.quageo.2011.03.001.

Saidi, A., Ghassemi, M. R., Aghanabati, A., Keyhani, E., Vakili, F., Golshani, F., Keshani, F., Bozorgania, F., Mohtat, T., Ezatian, F., Davari, M., & Baghdadi, I., 2003. Geological Map of Baladeh [Map]. Geological Survey of Iran.

Sanderson, D.J., Marchini, W.R.D., 1984. Transpression. J. Struct. Geol. 6 (5), 449–458. https://doi.org/10.1016/0191-8141(84)90058-0.

Sarkarinejad, K., Ansari, S., 2015. Did the 1983 Charazeh earthquake trigger the destructive 1990 Rudbar earthquake? Int. J. Earth Sci. 104 (1), 309–319. https://doi.org/10.1007/s00531-014-1072-z.

Selim, H.H., Tüysüz, O., Karakaş, A., Taş, K.Ö., 2013. Morphotectonic evidence from the southern branch of the North Anatolian Fault (NAF) and basins of the south Marmara sub-region, NW Turkey. Quat. Int. 292, 176–192. https://doi.org/10.1016/j.quaint.2012.11.022.

Şengör, A.M.C., Kidd, W.S.F., 1979. Post-collisional tectonics of the Turkish-Iranian plateau and a comparison with Tibet. Tectonophysics 55 (3–4), 361–376. https://doi.org/10.1016/0040-1951(79)90184-7.

Sheykholeslami, M. R., Javadi, H. R., Asadi, M., 2013. Iran Fault Map on Provincial Subdivisions [Map]. Geological Survey of Iran.
Sibson, R.H., 1977. Fault rocks and fault mechanisms. J. Geol. Soc. London 133 (3), 191–213. https://doi.org/10.1144/gsjgs.133.3.0191.
Sibson, R.H., 2003. Thickness of the Seismic Slip Zone. Bull. Seismol. Soc. Am. 93 (3), 1169–1178. https://doi.org/10.1785/0120020061.
Sodoudi, F., Yuan, X., Kind, R., Heit, B., Sadidkhouy, A., 2009. Evidence for a missing crustal root and a thin lithosphere beneath the Central Alborz by receiver function studies. Geophys. J. Int. 177 (2), 733–742. https://doi.org/10.1111/j.1365-246X.2009.04115.x.
Solaymani Azad, S., Ritz, J.F., Abbassi, M., 2011. Analysing the junction between the Mosha and the North Tehran active faults. Tectonophysics 497, 1–14.
Stöcklin, J., 1974. Possible ancient continental margins in Iran. In: Burk, C., Drake, C. (Eds.), The Geology of Continental Margins. Springer, Berlin Heidelberg, pp. 873–887. https://doi.org/10.1007/978-3-662-01141-6_64.
Takagi, H., Takahashi, K., Shimada, K., Tsutsui, K., Miura, R., Kato, N., Takizawa, S., 2012. Integrated estimates of the thickness of the fault damage zone in granitic terrain based on penetrative mesocracks and XRD analyses of quartz. J. Struct. Geol. 35, 64–77. https://doi.org/10.1016/j.jsg.2011.11.008.
Talebian, M., Copley, A.C., Fattahi, M., Ghorashi, M., Jackson, J.A., Nazari, H., Sloan, R. A., Walker, R.T., 2016. Active faulting within a megacity: the geometry and slip rate of the Pardisan thrust in central Tehran, Iran. Geophys. J. Int. 207 (3), 1688–1699. https://doi.org/10.1093/gji/ggw347.
Tatar, M., Hatzfeld, D., 2009. Microseismic evidence of slip partitioning for the Rudbar-Tarom earthquake (M_s 7.7) of 1990 June 20 in NW Iran. Geophys. J. Int. 176 (2), 529–541. https://doi.org/10.1111/j.1365-246X.2008.03976.x.
Tatar, M., Hatzfeld, D., Abbassi, A., Yamini-Fard, F., 2012. Microseismicity and seismotectonics around the Mosha fault (Central Alborz, Iran). Tectonophysics 544–545, 50–59. https://doi.org/10.1016/j.tecto.2012.03.033.
Tatar, M., Jackson, J., Hatzfeld, D., Bergman, E., 2007. The 2004 May 28 Baladeh earthquake (Mw 6.2) in the Alborz, Iran: overthrusting the South Caspian Basin margin, partitioning of oblique convergence and the seismic hazard of Tehran. Geophys. J. Int. 170 (1), 249–261. https://doi.org/10.1111/j.1365-246X.2007.03386.x.
Tavarnelli, E., Holdsworth, R.E., Clegg, P., Jones, R.R., McCaffrey, K.J.W., 2004. The anatomy and evolution of a transpressional imbricate zone, Southern Uplands, Scotland. J. Struct. Geol. 26 (8), 1341–1360. https://doi.org/10.1016/j.jsg.2004.01.003.
Tchalenko, J.S., 1975. Seismotectonic framework of the North Tehran Fault. Tectonophysics 29 (1–4), 411–420. https://doi.org/10.1016/0040-1951(75)90169-9.
Trifonov, V. G., Hessami, K., Popov, S. V., Zelenin, E. A., Trikhunkov, Ya. I., Frolov, P. D., Golovina, L. A., Simakova, A. N., Rashidi, A., Latyshev, A. V., 2022. Development of the Southern coastal area of the caspian sea during the pliocene–quaternary according to biostratigraphic and magnetostratigraphic data. Stratigr. Geol. Correl. 30(4), 273–291. https://doi.org/10.1134/S0869593822040074.
Tsereteli, N., Tibaldi, A., Alania, V., Gventsadse, A., Enukidze, O., Varazanashvili, O., Müller, B.I.R., 2016. Active tectonics of central-western Caucasus, Georgia. Tectonophysics 691, 328–344. https://doi.org/10.1016/j.tecto.2016.10.025.
Vernant, P., 2004. Deciphering oblique shortening of central Alborz in Iran using geodetic data. Earth Planet. Sci. Lett. 223 (1–2), 177–185. https://doi.org/10.1016/j.epsl.2004.04.017.
Vernant, P.h., Nilforoushan, F., Hatzfeld, D., Abbassi, M.R., Vigny, C., Masson, F., Nankali, H., Martinod, J., Ashtiani, A., Bayer, R., Tavakoli, F., Chéry, J., 2004. Present-day crustal deformation and plate kinematics in the Middle East constrained by GPS measurements in Iran and northern Oman. Geophys. J. Int. 157 (1), 381–398. https://doi.org/10.1111/j.1365-246X.2004.02222.x.
Walcott, R.I., 1984. The kinematics of the plate boundary zone through New Zealand: a comparison of short- and long-term deformations. Geophys. J. Int. 79 (2), 613–633. https://doi.org/10.1111/j.1365-246X.1984.tb02244.x.
Walker, R., Talebian, M., Saiffori, S., Sloan, R.A., Rasheedi, A., MacBean, N., Ghassemi, A., 2010. Active faulting, earthquakes, and restraining bend development near Kerman city in southeastern Iran. J. Struct. Geol. 32 (8), 1046–1060. https://doi.org/10.1016/j.jsg.2010.06.012.
Zarifi, Z., Nilfouroushan, F., Raeesi, M., 2014. Crustal stress map of iran: insight from seismic and geodetic computations. Pure Appl. Geophys. 171 (7), 1219–1236. https://doi.org/10.1007/s00024-013-0711-9.